Physics – Uspekhi **53** (11) 1123 – 1149 (2010)

REVIEWS OF TOPICAL PROBLEMS

PACS numbers: 12.38.Mh, **24.85.+p**, 41.60.Bq

IN MEMORY OF VITALY LAZAREVICH GINZBURG

The quark–gluon medium

I M Dremin, A V Leonidov

DOI: 10.3367/UFNe.0180.201011c.1167

Contents

Abstract. The properties of the quark–gluon medium observed in high-energy nucleus–nucleus collisions are discussed. The main experimental facts about these collisions are briefly described and compared with data about proton–proton collisions. Both microscopic and macroscopic approaches to their description are reviewed. The chromodynamics of the quark–gluon medium at high energies is mainly considered. The energy loss of partons moving in this medium is treated. The principal conclusion is that the medium possesses some collective properties which are crucial for understanding the experimental observations.

Foreword

It is a great honor for us to publish this paper in the volume dedicated to the memory of V L Ginzburg. His contribution to condensed matter physics crowned by the Nobel Prize is extremely important. Nowadays these ideas have become relevant for high-energy physics. The properties of the quark–gluon medium created in high-energy nucleus collisions (often called the quark–gluon plasma) are intensively studied. The first steps in the chromodynamics of quark–gluon matter are strongly reminiscent of those in the electrodynamics of continuous media, albeit with some visible differences.

I M Dremin, A V Leonidov Lebedev Physical Institute,
Russian Academy of Sciences,
Leninskii prosp. 53, 119991 Moscow, Russian Federation
Tel. (7-495) 783 37 19
E-mail: dremin@lpi.ru, leonidov@lpi.ru

Received 16 June 2010
Uspekhi Fizicheskikh Nauk **180** (11) 1167 – 1196 (2010)
DOI: 10.3367/UFNr.0180.201011c.1167
Translated by I M Dremin, A V Leonidov;
edited by A M Semikhatov

1. Introduction

The subject of *the quark–gluon medium* has become so broad that it deserves a series of monographs, even in spite of still being in the actively developing stage, and cannot be fully covered within a single review paper. That is why we mostly concentrate here on general ideas about the evolution of the quark–gluon medium in high-energy heavy ion collisions and on those properties of the medium that are revealed by the energy losses of partons moving in it. These properties are described by the chromodynamics of the quark–gluon medium, which is the main topic of this review.

Nevertheless, it would be too 'ostrich-like' a behavior not to mention imminent problems and approaches, and we therefore include brief discussions of some of them in this review. In particular, the similarities and differences between electrodynamic and chromodynamic processes are described. The extremely popular hydrodynamic approach has been widely discussed in many review papers, and we decided to give just a short description of it here, referring to the corresponding literature. The anti de Sitter/quantum chromodynamics (AdS/QCD) correspondence is touched upon only slightly. Lattice results are mentioned very briefly too. They are mostly applicable to the static properties of hadrons and are of interest to us here in relation to phase transitions. Very interesting ideas about possible local CP violation in heavy ion collisions are briefly mentioned but not discussed in detail. The relation of the little bang in heavy ion collisions to the Big Bang in cosmology is another topic of interest; however, it is out of the scope of our survey. A short overview

of experimental results is presented in Section 2. But in subsequent sections of this review, only those experimental papers are cited that are discussed in more detail in connection with theoretical considerations. We apologize to those whose work could not be completely reviewed due to the limited size of this paper.

The internal structure and interactions of particles and nuclei are the main goal of studies at accelerators. According to present knowledge, strong interactions are described by quantum chromodynamics (QCD), with quarks and gluons regarded as elementary objects (partons) responsible for the interaction.

At low energies, the partons are confined inside strongly interacting particles (hadrons) and determine their static properties. At high densities, we have the nonperturbative region of QCD describing the strongly interacting matter in thermal equilibrium at a finite temperature.

The matter produced in collisions is surely different from the one described above. Highly coherent parton configurations and strong internal fields become especially important. Collisions of heavy nuclei at ultrarelativistic energies are expected to produce a hot and dense internally colored medium. It should exhibit some collective properties different from those seen under static conditions. Low-momenta modes in nuclear wave functions can be described in terms of classical fields coupled to some high-momenta static color sources.

According to present knowledge, the collision process (energy evolution of all modes) proceeds through several stages. We discuss some of them at the beginning of the review. The corresponding equations describing these processes are also discussed. At one of the stages, quarks and gluons may become deconfined inside some finite volume during a short time interval. As far as we know, they form some ideal liquid. Its collective properties are revealed by its mechanical motion as a whole described by hydrodynamics, and by the chromodynamic response to partons penetrating it, described by in-medium QCD.

At large transferred momenta, the QCD coupling becomes small (asymptotic freedom) and the perturbative approach starts being applicable. Experiments with high-energy particle collisions are needed precisely to allow studying processes with high transferred momenta. In accordance with the uncertainty principle, this offers insights into the particle structure at ever smaller distances. In this way, the quark–gluon content of a particle, its scale dependence, and the properties of the interaction region are studied.

Moreover, the hard processes inside a medium may induce its collective coherent response. That would allow studying medium properties similarly to learning about Earth's structure through underground explosions. This is especially true at the highest energies because the parton densities inside colliding strongly interacting nuclei increase with energy. Therefore, the collective effects become pronounced and, in central heavy ion collisions, long-range correlations appear alongside short-range ones.

Experimental investigations into the properties of matter inside the interaction region require studying the energy losses of various trial partons moving in it. This is analogous to studies of energy losses of electrons passing through ordinary amorphous matter. Recent experimental results from the SPS (Super Proton Synchrotron) and RHIC (Relativistic Heavy Ion Collider) clearly show that the collective medium behavior becomes crucial in heavy ion collisions. The radiation properties of partons are modified and the energy spectra of final hadrons as well as their correlations are changed relative to those in pp collisions. The induced coherent emission reveals the collective response of the medium to partons penetrating it. The medium itself displays the collective motion. The hadrochemical content of produced particles changes. Both microscopic and macroscopic QCD approaches to the theoretical description of these findings are effective. The mechanical and thermodynamic properties of the medium are studied in the hydrodynamic approach. We describe all of them in what follows, and discuss the corresponding experimental data. Throughout this paper, we use the system of units in which $\hbar = c = 1$.

2. Main experimental findings

Nucleus–nucleus (AA) collisions are studied experimentally at the SPS and RHIC. The very first question addressed is the difference between AA and pp processes at high energies. Various characteristics have been measured and compared. They clearly show that nuclear collisions cannot be regarded as an incoherent superposition of nucleon–nucleon collisions. Some collective properties of the medium must be taken into account to explain the difference.

The yield of particles produced at rapidity y and large transverse momenta p_{T} is suppressed in AA relative to pp. This is demonstrated by plotting the nuclear modification factor R_{AA} for a single-inclusive hadron cross section:

$$R_{\mathrm{AA}}(y, p_{\mathrm{T}}; b) = \frac{\mathrm{d}N_{\mathrm{AA}}/\mathrm{d}y\,\mathrm{d}p_{\mathrm{T}}}{N_{\mathrm{part}}\,\mathrm{d}N_{\mathrm{pp}}/\mathrm{d}y\,\mathrm{d}p_{\mathrm{T}}}. \quad (1)$$

The factor R_{AA} measures the deviation of an AA reaction with the number N_{part} of participant nucleons (determined by the nuclear overlap function at the impact parameter b) from an incoherent superposition of pp reactions, for which $R_{\mathrm{AA}} = 1$. A similar expression can be written for the dihadron correlations (usually denoted by I_{AA}).

In both particle and heavy ion collisions, the production of soft momentum particles with the transverse momenta $p_{\mathrm{T}} < 2$ GeV strongly dominates. The corresponding spectrum decreases exponentially with the transverse kinetic energy $(p_{\mathrm{T}}^2 + m_i^2)^{1/2} - m_i$. The pion spectra are flatter in the AA collisions than in the pp ones. This is even more true for kaons and antiprotons, with the latter having the smallest slope. These spectra are used to determine the kinetic freeze-out temperature and the dependence of the transverse flow velocity on the energy and centrality (i.e., the degree of collectivity of the interaction).

Accordingly, soft pions dominate multiplicity distributions. Their shape is approximately described by negative binomial distributions in both particle and heavy ion collisions at high energies, although some deviations from them (predicted by QCD) are revealed by correlation measures such as their moments.

The shape of the charged hadron transverse momentum spectra changes at $p_{\mathrm{T}} \approx 3$ GeV from exponential to power-like as predicted by the perturbative QCD. This power-law tail affects a very small portion of particles. The RHIC results on single-particle inclusive distributions in central Au–Au collisions at the energy 200 GeV show a strong p_{T}-independent suppression, $R_{\mathrm{AA}} \approx 0.2$, of the hadronic yield at large $p_{\mathrm{T}} > 4$ GeV. The measurements covered the interval in p_{T} up

to 20 GeV. This striking deficit of particles with a high transverse momentum points to an energy loss of partons in the medium. It corresponds to the so-called jet quenching effect with the spectra of hadrons produced by partons in the medium softened compared to those in the vacuum. Therefore, this suppression factor is a powerful tool to map out the density of the medium.

The high-p_T suppression in Au–Au and Cu–Cu collisions is comparable at the same number of 'participants' N_{part} (nucleons that underwent at least one inelastic interaction). The ratio R_{AA} is closer to 1 for more peripheral collisions. It depends on the angular orientation of the high-p_T hadron with respect to the reaction plane (on the azimuthal angle). This dependence may be explained as being due to the dependence of the energy loss on the length traversed by the particle in the medium.

The ratio R_{AA} is independent of the hadron identity at high p_T. In electrodynamics, by contrast, the radiation of electrons is much stronger than that of muons. Interesting effects occur for suppression of spectra of charmed mesons and charmonium: the former are suppressed at the same level as pions, while the latter is suppressed at the same level as at the SPS energy $\sqrt{s} = 17$ GeV.

Another intriguing feature of the data is that direct photons do not seem to be suppressed in the region of p_T from 4 GeV to 15 GeV, while at very large $p_T \sim 20$ GeV, preliminary data show a suppression with $R_{AA} \approx 0.6$.

At smaller transverse momenta, $0.25 < p_T < 4$ GeV, the suppression effect is weaker, and R_{AA} even increases slightly at low $p_T < 3$ GeV. This is qualitatively explained by the parton rescattering in the initial state, which leads to the widening of the transverse momentum spectra (the Cronin effect). At the SPS energies, the results refer only to this domain of transverse momenta with larger values of R_{AA} than at RHIC. The SPS value (Pb–Pb at $\sqrt{s} = 17.3$ GeV) of R_{AA} at $p_T = 4$ GeV is much larger than at higher energies of the RHIC, exceeding 1 for $p_T > 2$ GeV (the strong Cronin effect). That is expected from the more important role of gluons compared to quarks at the RHIC ($C_A/C_V = 9/4$). For collisions with smaller dAu overlap at 200 GeV, the Cronin effect persists at least up to $p_T = 8$ GeV. Experimental data show that the suppression of inclusive spectra sets in somewhere between $\sqrt{s} \simeq 20$ GeV and $\sqrt{s} \simeq 60$ GeV. The dominating process of soft particle production is characterized by scaling with the number of participants rather than with the number of binary collisions typical for hard processes.

Correlations among secondary particles are a more sensitive instrument in distinguishing between model predictions than the single-particle inclusive data. The study of correlations has revealed many exciting features. The most spectacular of them refer to jets produced in the processes in which a high-p_T particle is present. If a high-p_T particle is chosen as a trigger and other hadrons are measured within a circle surrounding it[1] defined by the (pseudo)rapidity + azimuthal angles in the plane orthogonal to the momentum of the initial particle, then the Gaussian-like structure around the trigger (the near-side jet) is usually seen in pp reactions. Moreover, both two- and three-particle correlations show two back-to-back jet-like peaks (dijet production). Theoretically, jets are considered, in the first approximation, as surviving remnants of hard-scattered quarks and gluons.

In AA collisions, jets are expected to widen in angles and the momentum spectra of their particles are expected to soften. This phenomenon is termed jet quenching. A quantitative analysis of jet quenching in heavy ion collisions requires model building. So far, there are many uncertainties in their predictions. Also, biases are introduced by some experimental jet selection criteria. To reduce the dependence on these effects, different triggers (e.g., γ and π^0) were used and the away-side hadron spectra were measured.

Correlations of nonphotonic electrons from charm and bottom decays with hadrons are different for jets with D and B mesons.

Multiparticle correlations and fully (calorimetrically) reconstructed jets are the main goals of recent efforts in the studies of pp and AA collisions. The first results for fully reconstructed jets in pp, Cu–Cu, and Au–Au collisions clearly demonstrate that jets are broadened in the quark–gluon medium. In general, the color connections of jets to the bulk or, for example, to beam remnants in W + jet events, and the event-by-event analysis of color flows are also important. The first experimental hints of intrajet broadening due to such color flows in them have been obtained.

The influence of jet quenching and background fluctuations on conclusions about jet fragmentation functions is actively being studied now. Surprisingly enough, no modification of them in AA collisions compared to the pp ones has been observed at high p_T in preliminary studies. This may show that a biased jet population was selected (surface effect?), and jet selection criteria should be modified.

Even more surprising were observations of completely new topologies called ridge and double-humped events in AA collisions. In central collisions, the near-side jet happens to stand on the pedestal (ridge) with a long extension in measured pseudorapidities up to $|\eta| = 4$, steeply decreasing in the azimuthal direction. The presence of the ridge is independent of the jet peak. The characteristics of this peak are the same as those of bulk particle production. However, the particle spectrum in the ridge is somewhat harder than in the bulk. Moreover, this structure is also seen in two-particle correlations without a jet trigger. These events include all charged hadrons with $p_T > 150$ MeV. The event-by-event three-particle correlation studies on central collisions at higher $p_T > 1$ GeV showed that the particles from the ridge are uncorrelated in pseudorapidity both among themselves and with particles in the peak. The production of the ridge is uncorrelated with jet-like particle production. The ridge disappears in low-multiplicity peripheral collisions and at high p_T of the trigger particle. Both the long pseudorapidity extension of the ridge and the large wide clusters found in two-particle correlations point to the important role of collective effects.

The away-side peak at $\Delta\phi = \pi$ is present in pp collisions, but is replaced by a broad away-side structure in Au–Au collisions. The two symmetric maxima (humps) are clearly seen in most central collisions at $\Delta\phi \approx \pi \pm 1.1$. They are resolved after the flow effects are subtracted and contain hadrons with small energies. The peak positions are approximately independent of the transverse momenta of the trigger and associated particles. The peak heights slowly increase with p_T^{trig} at fixed p_T^{assoc}. The two humps seem to merge into a single wide hump at large p_T of the trigger ($6 < p_T^{trig} < 10$ GeV), indicating the reappearance of the

[1] Besides such a cone algorithm, the recombination algorithms with iterative pairing of nearby particles and simple Gaussian filtering are very widely used. These algorithms are helpful in separating jets from the background.

away-side jet just between these humps, as it should be in a finite-size medium where the parton with extra p_{T} goes outside it in the form of a jet. The heavy quark jets have similar qualitative features (although measured with fewer statistics). These peculiar features are seen in both two- and three-particle correlations. They evidence a conical emission pattern. The existence of these features is certainly related to collective properties of the medium. In mid-central collisions, the maximum position is shifted for some special choices of the trigger location relative to in-place and out-of-plane directions. This special feature can be explained by the effect of the wake (see below).

The associated yield of away-side hadrons is suppressed at large p_{T} in Au–Au collisions relative to the pp ones, albeit less than the single-particle spectrum ($I_{\mathrm{AA}} \approx 0.35 - 0.56$ while $R_{\mathrm{AA}} \approx 0.2$).

Two-particle correlations between charged hadrons generated by final-state Coulomb interactions provide valuable information. Also, Bose–Einstein (BE) correlations between pairs of identical bosons caused by quantum symmetrization of wave functions are studied with the help of interferometry à la Hanbury Brown–Twiss (HBT). They are observed as an enhancement of pairs of same-sign charged pions at small relative momenta and tell us about the space–time structure and evolution of the source. In central collisions at mid-rapidity, three radii R_{long}, R_{out}, and R_{side} are usually reconstructed from measurements. They are respectively directed along the beam direction, the direction of the emission of the pair $\mathbf{p}_{\mathrm{T}}$, and the direction perpendicular to these two. Within experimental errors, all the three radii turn out to be equal and rather steeply decreasing with transverse momenta. This contradicts the hydrodynamic predictions and is therefore called the 'RHIC HBT puzzle.' Moreover, recent data show that the HBT characteristics of pp collisions behave similarly to those of AA, which adds new questions to this puzzle. The size of the correlated particle emission region increases with the particle multiplicity in the event. The number of radii is larger (six) for noncentral collisions. They increase with the number of participants and exhibit oscillations as functions of the azimuthal angle. The growth rate decreases with transverse momenta (as do the radii themselves). The amplitude of oscillations is larger for more peripheral collisions and vanishes in central collisions.

A modified shape of bosonic resonances created in nuclear collisions has been observed. In all cases, the traditional Breit–Wigner form acquires an excess in its low-energy wing, as is revealed in mass correlations of the decay products.

Collective flows of final particles present another interesting effect. These flows are generated by the internal pressure in the quark–gluon medium. Their shapes are determined by spatial characteristics of the initial overlap volumes and by the interaction dynamics. The azimuthal angle distribution of the emitted particles can be written as

$$E\frac{\mathrm{d}N}{\mathrm{d}^3p} = \frac{1}{2\pi}\frac{\mathrm{d}N}{\mathrm{d}y p_{\mathrm{T}}\,\mathrm{d}p_{\mathrm{T}}}\left(1 + \sum_{n=1}^{\infty} 2v_n \cos\left[n(\phi - \Psi_r)\right]\right), \quad (2)$$

where Ψ_r denotes the reaction (event) plane determined, independently for each component, from the flow itself: $v_n = \left\langle \cos\left[n(\phi - \Psi_r)\right]\right\rangle$ with averaging over all particles in all events as indicated by the angle brackets. The first harmonic coefficient of the Fourier expansion of azimuthal distributions, v_1, describes the isotropic radial flow, and the second coefficient, v_2, characterizes the elliptic flow. The azimuthal asymmetry of particle distribution with respect to the reaction plane defined by the beam direction and the impact parameter vector corresponds to the anisotropic flow. Higher harmonics are also being studied. The 'nonflow' contributions due to the jets, the ridge, resonance decays, and HBT effects are usually subtracted.

The radial flow manifests itself in a flattening (in AA collisions compared to pp ones) of the spectra at a small transverse kinetic energy, the flattening being stronger for heavier particles. It scales with the energy and the system size. This effect is more pronounced in central collisions between equal spherical nuclei. The change of sign of the radial flow of protons (the so-called 'wiggle') as a function of rapidity for most peripheral events at SPS energies has been noticed. No wiggle has been observed at the RHIC. The coefficient v_1 stays negative (antiflow) and steadily increasing for all pseudorapidities; this shows the early start of collective effects.

The most intensively studied elliptic flow is related, first of all, to the noncentrality of collisions (the spatial eccentricity of the reaction zone) and to the rescattering of partons. The elliptic shape of the overlap region gives rise to different pressures in different directions and therefore to nonzero v_2. Thus, the coefficient v_2 is sensitive to the system evolution at very early times. The integrated elliptic flow increases with the energy. This increase is stronger in more central collisions than in mid-central ones, while the absolute values are smaller. The value of v_2 depends on the pseudorapidity with a maximum at $\eta = 0$ and increases with the energy. It decreases by about a factor of two around $\eta = 3$. The value of v_2 is smallest for more central collisions. The dependence on the transverse momentum has been measured up to $p_{\mathrm{T}} = 12$ GeV, showing a maximum at about $p_{\mathrm{T}} = 3$ GeV with v_2 becoming as large as 0.2, which is followed by some saturation or slow decrease. At $p_{\mathrm{T}} < 2$ GeV, v_2 is characterized by scaling with the transverse kinetic energy $m_{\mathrm{T}} - m$ and at $2 < p_{\mathrm{T}} < 4$ GeV, with the number of constituent quarks. The relation of v_2 to the spatial eccentricity of an event depends on the number of participants (system size). The coefficient v_2 has been measured for different particle species. The baryonic elliptic flow saturates at somewhat higher p_{T} and larger v_2 values than for mesons. The value of v_2 is close to 0 for J/ψ in Au–Au collisions at 200 GeV.

Enhancement of the yield of various particle species at high p_{T} in AA collisions compared to the very strong suppression of pions has been observed. In particular, the hadrochemical compositions in AA and pp collisions are different. This is considered to be a manifestation of the quark–gluon plasma (or, more generally, of the prehadronic state) effects. Neutral pions and η-mesons at high $p_{\mathrm{T}} > 2$ GeV are strongly suppressed (by about 5 times) in central AA collisions relative to pp processes. The suppression of ϕ mesons is the same at high $p_{\mathrm{T}} > 5$ GeV, but is smaller in the intermediate range $2 < p_{\mathrm{T}} < 5$ GeV. No suppression is seen for photons in this kinematic range. Proton production is enhanced at intermediate $p_{\mathrm{T}} \approx 2-5$ GeV, with the p/π ratio approaching unity. Quite surprising is the fact that in AA at the RHIC, antiprotons are as abundant as negative pions for $p_{\mathrm{T}} > 2$ GeV. That is probably related to the collective transverse flow. In particle collisions, the strange particle production at high p_{T} is strongly suppressed compared to pions (3–4 times), but is enhanced by about a factor of two in AA processes such that the suppression factor becomes about 0.6– 0.7. The enhancement is larger for particles with higher strangeness content,

such as Ξ and Ω. The overall fraction of strange particles is about twice as high in heavy ion collisions compared to elementary particle collisions. A similar relatively small suppression factor was measured for charmed quarks (J/ψ). The upper limit 0.64 for bottom (Υ) suppression was recently obtained. A strong suppression of high-p_T electrons originating from the decays of charm and beauty hadrons indicates the same value of suppression for heavy and light quarks in the quark–gluon medium. This shows that the initial stage of creation of highly virtual quarks is more important than their subsequent mass difference. The change in the hadrochemical content of collision products with high p_T may reflect a difference in in-medium interactions of the species and requires taking the collective (nonlocal) properties of the medium into account (with possible diffusion before hadronization).

Remarkably enough, at very low $p_T < 0.5$ GeV of secondary particles, their yields seem to be the same in pp, AA, and even e^+e^- processes (albeit different for different species) and independent of the primary energy, as is expected from the universality of coherent processes for long-wavelength gluons.

The above statements can be illustrated by numerous figures that can be found in experimental presentations and more specialized review papers. We only show some of them to elucidate theoretical argumentation, thus keeping this article within reasonable size.

All these observations are closely related to the general physical process of the energy loss of partons during collisions of nuclei, which is to a large extent the topic of this review.

3. Microscopic description of the quark–gluon medium

Evidently, the microscopic QCD description of all processes with thousands of particles produced is impractical in the whole phase space region. Such a description may be applicable to relatively rare high-p_T subprocesses where the QCD coupling constant becomes smaller. For soft partons and hadrons, the rescattering and hadronization effects are too strong to leave many traces of the primary inelastic process. The macroscopic approach (including the statistical one) is more suitable for a description of purely collective medium effects.

It is nevertheless possible to follow the general evolution of fields during heavy ion collisions and reveal typical correlation patterns by applying the main principles of QCD. In this context, the present paradigm, which we describe below, pictures a transition from the color glass condensate (CGC) to Glasma, eventually evolving into quark–gluon plasma (QGP) and subsequent hadronization.

The energy loss of partons in the quark–gluon medium is the main source of experimental information about its properties during these stages. As in electrodynamics, it may be separated into two categories.

The loss due to a change in the velocity vector of a parton such as elastic scattering, bremsstrahlung, or synchrotron radiation is usually treated microscopically. All these phenomena result from a *short-range* response of the parton to the impact of matter fields. Elastic scattering does change the parton energy due to the recoil effect and deflects it, thus changing the energy flow in the initial direction. At high energies, this process is less probable than the emission of gluons (bremsstrahlung) due to nearby collisions with the matter constituents. The medium structure imposes some restrictions on the coherence properties of the radiation process and on the effective radiation length (in analogy to the Ter-Mikhaelyan and Landau–Pomeranchuk effects in electrodynamics). In the general case, the intensity of the radiation depends on the relation of the path length of the parton in the medium, its mean free path (depending on the distance between the scattering centers and on the cross section), and the formation length of emitted radiation. The synchrotron radiation of gluons induced by the curvature of the parton trajectory in chromomagnetic fields may become important for sufficiently strong fields. These processes are considered in Section 3.

A principally different source of energy losses is associated with medium polarization by a propagating parton. Here, one speaks about the collective response of the medium related to the nonperturbative *long-range* interconnection of its constituents described by its chromopermittivity. This is treated macroscopically within the in-medium QCD. The corresponding effects are analogous to Cherenkov radiation, the wake, and the transition radiation. In these processes we can in the first approximation neglect the change in the velocity vector of the parton. The macroscopic aspect of the problem is sometimes ignored in review papers, and we discuss it in more detail in Section 4.

We note that the total energy loss is the sum of the losses due to short-range and long-range interactions.

3.1 Color glass condensate, glasma, and quark–gluon plasma

Is it possible to work out a quantitative description of multiparticle production in hadronic and nuclear collisions within QCD? An ambitious attempt to answer this question is provided by the paradigm of color glass condensate (CGC); see, e.g., reviews [1–4]. In the words of one of the principal creators of this paradigm, "Color Glass Condensate is a universal form of matter which controls the high energy limit of all strong interaction processes and is the part of the hadron wavefunction important at such energies" [5].

The strength of the CGC approach to the physics of high-energy scattering lies in providing a unifying concept for such important but previously separately existing notions as soft (wee) and constituent partons, stringy and jetty particle production, structure functions, limiting fragmentation, etc.

Multiparticle production in QCD is generated by low-x partons in the nuclear wavefunctions (CGC). Chromoelectric and chromomagnetic fields in the medium under consideration are the strongest fields in nature. When two 'pancakes' of CGC collide, they form matter with a very high density, called Glasma. It precedes the quark–gluon plasma (QGP). Glasma consists of color flux tubes localized in the transverse plane and stretching between the valence color degrees of freedom. These tubes generate long-range correlations responsible for flat distributions in the pseudorapidity $\Delta\eta$. The existence of long-range (pseudo)rapidity correlations is related to the early times of Glasma formation in nuclear collisions $\tau \leqslant \tau_{\text{out}} \exp(-|y_a - y_b|/2)$, where τ_{out} is the proper time of production of particles a and b with rapidities y_a and y_b. The radial flow collimates particles in the direction of the flow and generates azimuthal correlations but does not affect the distribution over $\Delta\eta$. Notably, the ridge can be explained as the combination of the initial-state long-range rapidity correlations and the final-state radial flow. Therefore, combined elements of both the micro- and macro-approaches are necessary to explain the ridge phenomenon.

Color glass condensate is an effective theory describing hadronic and nuclear wavefunctions in the regime where the main contribution to the cross section comes from their multiparton Fock components, i.e., in essence, from dense gluon matter. The key idea behind the physical picture of CGC can be formulated as follows. We consider a fast hadron (nucleus) moving along the z axis with a large longitudinal light-cone momentum P^+. The modes in the projectile are classified by their relative yields of longitudinal momenta $x = p^+/P^+$. From the uncertainty relation, the characteristic longitudinal extension of these modes is $\Delta x^- \sim 1/(xP^+)$ and their characteristic lifetime is $\Delta x^+ \sim 1/p^- \simeq 2xP^+/m_\perp^2$,[2] where $m_\perp^2$ is some characteristic scale of the transverse momentum. We see that the hard constituent modes, for which $x \sim 1$, are localized at small distances and have large lifetimes, while the soft wee modes, for which $x \ll 1$, are spread over large longitudinal distances and are short lived. From the data on structure functions from deep inelastic scattering, we know that the number of wee partons, most importantly gluons, rapidly increases with $1/x$, $xG(x, Q^2) \sim (1/x)^\varkappa$ with $\varkappa \simeq 0.3$, and hence these modes are characterized by large occupation numbers. For such modes, it is natural to replace the language of particles by that of fields, and, in turn, the appropriate description for coherent multiparticle states is in terms of *classical* fields.

These considerations lie at the origin of the McLerran–Venugopalan model of nuclear light-cone wavefunctions [6–8] in which, in the framework of QCD, the constituent and wee partons are integrated in the unifying picture with the strongly localized slowly evolving constituent hard modes regarded as the *source* for the delocalized soft wee gluon field for which nonlinear effects must be taken into account, leading, in particular, to the saturation of the gluon distribution (see below).

We introduce the variables to be used in this section. Most of the formulas are written in terms of light-cone coordinates. For the four-vector $x^\mu = (t, \mathbf{x}_\perp, z)$, the $\pm$-components are defined as

$$x^\pm = \frac{t \pm z}{\sqrt{2}}. \tag{3}$$

The momentum components are described analogously. We also extensively use the (τ, η) coordinate system

$$\tau = \sqrt{2x^+x^-}\,, \quad \eta = \frac{1}{2}\ln\frac{x^+}{x^-}\,, \tag{4}$$

where τ is the proper time and η is the spatial rapidity.

3.1.1 McLerran–Venugopalan model. Saturation. To illustrate the machinery of the McLerran–Venugopalan model, we consider a calculation of the momentum space density of gluon modes

$$\frac{\mathrm{d}N}{\mathrm{d}^3k} = \left\langle a_\mathrm{c}^{i\dagger}(x^+, \mathbf{k})\, a_\mathrm{c}^i(x^+, \mathbf{k})\right\rangle = \frac{2k^+}{(2\pi)^3}\left\langle A_a^i(k, x^+)\, A_a^i(-k, x^+)\right\rangle, \tag{5}$$

from which the observable gluon structure function can be calculated as

$$xG(x, Q^2) = \int^{Q^2} \mathrm{d}^2\mathbf{k}_\perp k^+ \left.\frac{\mathrm{d}N}{\mathrm{d}k^+\,\mathrm{d}^2\mathbf{k}_\perp}\right|_{x=k^+/P^+}. \tag{6}$$

[2] The light-cone coordinates x^+ and x^- are defined below in Eqn (3).

As long as we are interested in the high-density regime, the gauge potentials $A_a^i(k, x^+)$ in (5) correspond to soft wee gluon fields.

Calculating the momentum space gluon density in (5) requires specifying the gluon fields $A_a^i(k, x^+)$ and the nature of averaging. The first task is achieved by assuming that $A_a^i(k, x^+)$ satisfy the *classical* Yang–Mills equations with the source originating from hard constituent modes,

$$\left[D_\mu, F^{\mu\nu}\right] = \delta^{\mu+}\rho_1(\mathbf{x}_\perp, x^-)\,, \tag{7}$$

where $F^{\mu\nu} = \left[D^\mu, D^\nu\right]$ is the non-Abelian field strength and $D^\mu = \partial^\mu - \mathrm{i}gA^\mu$. The solution of (7) is conveniently written in the light-cone gauge $A^+ = 0$. It is easy to verify that for a static x^+-independent solution, $A^- = 0$, and hence the solution of (7) is purely transverse:

$$A^i(\mathbf{x}_\perp, x^-) = \frac{\mathrm{i}}{g}\, U(\mathbf{x}_\perp, x^-)\,\partial^i U^\dagger(\mathbf{x}_\perp, x^-)\,, \tag{8}$$

where

$$U(\mathbf{x}_\perp, x^-) = P\exp\left\{\mathrm{i}g\int_{-\infty}^{x^-}\mathrm{d}y^-\alpha(\mathbf{x}_\perp, x^-)\right\}, \tag{9}$$

and $\alpha(\mathbf{x}_\perp, x^-) = -\rho(\mathbf{x}_\perp, x^-)/\nabla_\perp^2$ is the solution of (7) in the covariant gauge. Solution (8), (9) is a nonlinear functional of the color charge density $\rho(\mathbf{x}_\perp, x^-)$ and, being exact, is nevertheless formal.

The second crucial step is related to specifying the nature of averaging in (5). The idea in [6–8] was that for a large nucleus and the transverse resolution of the probe $|\Delta\mathbf{x}_\perp| \ll 1/\Lambda_\mathrm{QCD}$, where Λ_QCD is the fundamental scale of strong interactions, $\Lambda_\mathrm{QCD} \sim 100$ MeV, the color density $\rho(\mathbf{x}_\perp, x^-)$ is, on an event-by-event basis, essentially a random function. In the simplest setting where the hard modes are constituent quarks, the static color density is just the total color charge of all constituent quarks that happen to lie in the tube under consideration. The averaging procedure in (5) is thus specified by some functional $W_{\Lambda^+}[\,\rho]$, where Λ^+ is the scale separating the hard modes from the soft ones. A simple but quite realistic averaging is provided by the Gaussian ensemble, with [3]

$$\left\langle \rho^a(\mathbf{x}_\perp, x^-)\,\rho^b(\mathbf{y}_\perp, y^-)\right\rangle_{W_{\Lambda^+}} = g^2\mu_A^2\,\delta^{ab}\delta^2(\mathbf{x}_\perp - \mathbf{y}_\perp)\,\delta(x^- - y^-)\,.$$

In the simplest case where the sources are constituent quarks, the factor μ_A^2 setting the scale for the transverse density of color charge is simply $\mu_A^2 = g^2A/(2\pi R_A^2)$ and is therefore proportional to $A^{1/3}$ (see, e.g., a detailed derivation in [1]). The color charge density μ_A is directly related to the physical saturation scale Q_s to be defined below, $Q_\mathrm{s} \approx 0.6\, g^2\mu_A$ [10].

It is convenient to present the expression for the gluon density (5) resulting after averaging over the stochastic sources ρ with the above Gaussian weight for the gluon density in transverse space $\varphi(x, \mathbf{k}_\perp^2)$[4]

$$\varphi(x, \mathbf{k}_\perp^2) = \frac{4\pi^3}{N_\mathrm{c}^2 - 1}\,\frac{1}{\pi R_A^2}\,\frac{\mathrm{d}N}{\mathrm{d}\ln(1/x)\,\mathrm{d}^2\mathbf{k}_\perp}\,. \tag{10}$$

[3] For a detailed analysis supporting this assumption, see [9].

[4] The convenience of introducing $\varphi(x, \mathbf{k}_\perp^2)$ lies notably in the fact that the quantum evolution of gluon distributions considered below is most naturally written precisely in terms of this so-called unintegrated structure function.

The characteristic properties of the resulting distribution can be conveniently presented by writing its asymptotic expressions as $\mathbf{k}_\perp^2 \to 0$ and $\mathbf{k}_\perp^2 \to \infty$:[5]

$$\varphi(x,\mathbf{k}_\perp^2)\big|_{\mathbf{k}_\perp^2\to\infty} \simeq \frac{1}{\alpha_s N_c}\,\frac{Q_s^2}{\mathbf{k}_\perp^2} \equiv \frac{\mu_A^2}{\mathbf{k}_\perp^2}\,,$$
$$\varphi(x,\mathbf{k}_\perp^2)\big|_{\mathbf{k}_\perp^2\to 0} \simeq \frac{1}{\alpha_s N_c}\,\ln\frac{Q_s^2}{\mathbf{k}_\perp^2}\,. \qquad (11)$$

The most important ingredient of (11) is the so-called saturation scale $Q_s^2 \sim A^{1/3}$. The A-dependence of Q_s^2 is directly related to that of μ_A^2.

The remarkable phenomenon of the gluon distribution flattening at small transverse momenta seen in (11) is called saturation. We see that saturation is characteristic of the regime in which the gluon density $\varphi \sim 1/\alpha_s$ is parametrically large. Another crucial observation that is of great significance for developing the quantum theory of gluon distributions is that the saturation scale becomes large at large A: $Q_s^2 \gg \Lambda_{\rm QCD}^2$. Because the saturation momentum Q_s sets the scale for all the transverse momenta in the problem, the theory is in the weak-coupling regime for an asymptotically large nucleus.

3.1.2 Glasma. In Section 3.1.1, in the CGC framework, we described the distribution of gluons inside the nucleus. With this knowledge, we can consider the problem of particle production in high-energy nuclear scattering. The main idea of the CGC-motivated approach to this problem is that once gluon distributions in nuclei before the collision are most naturally described in terms of fields, it makes complete sense to describe the energy and particle flux created at the early stage of these collisions also in terms of the gluon field. In the tree-level approximation, this amounts to solving the Yang–Mills equations with two external currents $\rho_{1,2}(\mathbf{x}_\perp, x^-)$ representing color distributions of the two incident nuclei propagating along $x^\pm = 0$:

$$\left[D_\mu, F^{\mu\nu}\right] = \delta^{\mu+}\rho_1(\mathbf{x}_\perp, x^-) + \delta^{\mu+}\rho_2(\mathbf{x}_\perp, x^-)\,. \qquad (12)$$

If we are interested in calculating the gluon production in the central region, where their rapidity distribution can be considered approximately flat, it is natural to seek a boost-invariant solution of (12) in the form [11]

$$A^i = \theta(-x^+)\,\theta(x^-)\,A^i_{(1)} + \theta(x^+)\,\theta(-x^-)\,A^i_{(2)} + \theta(x^+)\,\theta(x^-)\,A^i_{(3)}\,,$$
$$A^\eta = \theta(x^+)\,\theta(x^-)\,A^\eta_{(3)}\,,$$

where $A^i_{(1,2)}$ are the gluon fields of the two incident nuclei before the collision described by (8) and $A^i_{(3)}$ and $A^\eta_{(3)}$ are the gluon fields created after the collision, which is assumed to occur at $\tau = 0$. Taken at the proper time $\tau = 0^+$, these fields describe the initial conditions for the subsequent evolution of dense matter created in high-energy nuclear collisions.

It is straightforward to verify that to ensure the matching of a solution of (12) at $\tau = 0$, the following relations must be satisfied:

$$A^i_{(3)}|_{\tau=0} = A^i_{(1)} + A^i_{(2)}\,,$$
$$A^\eta_{(3)}|_{\tau=0} = \frac{ig}{2}\left[A^i_{(1)}, A^i_{(2)}\right]. \qquad (13)$$

A crucial observation [12, 13] following from boundary conditions (13) is that at $\tau = 0^+$, there exist only longitudinal fields

$$E^z = ig\left[A^i_{(1)}, A^i_{(2)}\right],$$
$$B^z = ig\epsilon^{ij}\left[A^i_{(1)}, A^j_{(2)}\right], \qquad (14)$$

in which the energy created in the collision is stored. Hence, a major rearrangement of the structure of the solution occurs, i.e., the transition from the two transverse fields $A^i_{(1,2)}$ described in the CGC framework at $\tau = 0^-$ to the purely longitudinal chromoelectric and chromomagnetic fields immediately after the collision at $\tau = 0^+$, called glasma. We emphasize that, as is obvious from (14), the effect is purely non-Abelian. Because the only scale in the problem is the saturation scale Q_s, the correlation length in the impact parameter plane is $R_\perp \sim 1/Q_s$. Therefore, the physics is that of the longitudinal fields characterized by the transverse correlation radius $R_\perp$, i.e., a set of chromoelectric and chromomagnetic cylindrical tubes. It is at this point that the CGC description matches the old paradigm of high-energy hadronic collisions, the Lund string model. An important new ingredient, however, is the presence of *chromomagnetic* flux tubes. The very fact that $\mathbf{EB} \neq 0$ opens up a principal possibility of local CP violation [13].

In the course of subsequent evolution, the initial configuration of longitudinal fields undergoes a partial transformation into that also containing a transverse field, and the energies stored in longitudinal and transverse modes become approximately equal at $\tau \sim 1/Q_s$ [13].

The expressions for the number of initially produced gluons and their transverse energy can be written based on dimensional reasons:[6]

$$\left.\frac{dN}{d\eta}\right|_{\eta=0} = c_N\,\frac{\pi R_A^2 Q_s^2}{\alpha_s(Q_s)}\,,\quad \left.\frac{dE_\perp}{d\eta}\right|_{\eta=0} = c_E\,\frac{\pi R_A^2 Q_s^3}{\alpha_s(Q_s)}\,, \qquad (15)$$

where the coefficients $c_N \approx 0.1/4\pi$ and $c_E \approx 0.05/4\pi$ (see, e.g., [15] and the references therein) are determined from numerical solutions of (12).

More specifically, with the value of Q_s determined from the analysis of deep inelastic scattering at HERA for $x_{\rm eff} \sim 0.01$, as is appropriate for nuclear scattering at the RHIC, $Q_s({\rm RHIC}) \simeq 1.2\,{\rm GeV}$, it follows from (15) that the rapidity densities of the number of gluons and of the transverse energy are:

$$\left.\frac{dN}{d\eta}\right|_{\eta=0} \approx 1100\,,\qquad \left.\frac{dE_\perp}{d\eta}\right|_{\eta=0} \approx 500\ {\rm GeV}\,, \qquad (16)$$

which agrees with the experimental data. This can be interpreted as an indication of almost perfectly ideal isentropic evolution from the initial glasma phase, through the intermediate QGP stage, to that of the flux of final hadrons.

3.1.3 Glasma instabilities. In Section 3.1.2, we considered a boost-invariant solution of classical Yang–Mills equations (12) describing the conversion of two initial gluon fields inside the incident nuclei into the physical fields created in the

[5] For details of this calculation see, e.g., [1].

[6] Because of the ultraviolet divergence at $\tau = 0$, these quantities can meaningfully be computed only at nonzero $\tau > 0$ [14].

collision. These last fields can be described as a set of chromoelectric and chromomagnetic flux tubes having radii of the order of the inverse saturation momentum Q_s stretched between the receding sources.

In general, classical solutions of the Yang–Mills equations are expected to be unstable with respect to quantum fluctuations. For example, constant chromoelectric fields are unstable with respect to Schwinger gluon pair production and static chromomagnetic fields are characterized by the Nielsen–Olesen instability. A tree-level iterative calculation of gluon production in collisions of non-Abelian charges in [16] has also demonstrated the instability of the approximate tree-level solution with respect to higher-order corrections.

Therefore, it is probably not too surprising that the evolving glasma fields are unstable with respect to rapidity-dependent fluctuations. Such fluctuations are inevitable when quantum fluctuations are taken into account. An explicit calculation of the wavefunction of two colliding nuclei demonstrating this effect was done in [17].

In describing the corresponding instabilities, it is convenient to consider two regimes:

• Small proper times $\tau < 1/Q_s$. This is a regime in which the instabilities are those related to fields.

• Intermediate times $\tau > 1/Q_s$. This regime can be described in dual terms of fields and particle kinetics (see [18]).

The analysis of these instabilities was brought to a new level in the all-order numerical calculations made in [19, 20], where it was shown that the amplitudes of the soft modes increase as $\exp(\sqrt{\tau})$. An analysis of instabilities with respect to quantum fluctuations in the flux tube picture was performed in [21].

The physical origin of these instabilities is still under debate.

The closest known analogy is the non-Abelian Weibel instability [22–24], with both electric and magnetic type plasma instabilities developing in nonequilibrium plasmas with inhomogeneous distributions of particles in momentum space. The analogy to glasma is very natural because, as described above, the initially created configuration of glasma fields is maximally anisotropic (the initial transverse momentum is equal to zero).

The analysis in [24] has led to the total revision of the previously existing picture of particle production in nuclear collisions given in the framework of the so-called 'bottom-up' scenario of thermalization of the glue initially freed at the momentum scale Q_s, described in [25]. The reason for the revision was that instabilities are much more effective in producing soft gluons and driving the system towards isotropy faster than the bremsstrahlung mechanism considered in [25]. The new versions of the 'bottom-up' scenario notably include mechanisms of cascade turbulent-like multiplication of gluons [26–28].

3.1.4 Quantum evolution. High-energy factorization. The McLerran–Venugopalan model is by construction adequate for moderate values of the fractional light-cone momentum $x = k^+/P^+$. The quantum corrections to the tree-level correlators like (7) involve soft gluon emission and virtual gluon loops. Both effects bring in contributions that are parametrically of the order $O(\alpha_s \log(1/x))$. Because physical quantities cannot depend on an arbitrary separation scale of soft and hard modes $\log(\Lambda^+/P^+)$, there arises a Wilsonian renormalization group resumming such contributions. For dense gluon systems, this resummation of small-x enhanced terms has to include contributions through all orders in the gluon density. The logarithmic nature of quantum corrections makes it natural to use the rapidity variable $Y = \log(1/x)$. In these terms, for example, the gluon two-point function (5) can be interpreted as an average of the product of classical fields taken at some specified rapidity scale:

$$\langle AA \rangle_Y = \int \mathcal{D}\rho \, W_Y[\rho] \, A_{\rm cl}(\rho) \, A_{\rm cl}(\rho) \,. \tag{17}$$

The Wilsonian RG equation (the Jalilian–Marian-Iancu–McLerran–Leonidov–Kovner (JIMWLK) evolution equation [29–31]) is most naturally written as an equation for the functional $W_Y[\rho]$. As shown in [32], it can be rewritten in an elegant Hamiltonian form,

$$\frac{\partial W_Y[\rho]}{\partial Y} = \mathcal{H}[\rho] \, W_Y[\rho] \,, \tag{18}$$

where $\mathcal{H}[\rho]$ is the JIMWLK Hamiltonian

$$\mathcal{H}[\rho] = \frac{1}{2} \int_{\mathbf{x}_\perp, \mathbf{y}_\perp} \chi(\mathbf{x}_\perp, \mathbf{y}_\perp) \, \frac{\delta^2}{\delta\rho(\mathbf{x}_\perp) \, \delta\rho(\mathbf{y}_\perp)} + \int_{\mathbf{x}_\perp} \sigma(\mathbf{x}_\perp) \, \frac{\delta}{\delta\rho(\mathbf{x}_\perp)} \,. \tag{19}$$

In Eqn (19), the functions $\chi(\mathbf{x}_\perp, \mathbf{y}_\perp)$ and $\sigma(\mathbf{x}_\perp)$ are explicitly calculable [29–31] and correspond to the effects due to the respective emission of real and virtual gluons.

A remarkable identity relating the real and virtual kernels $\chi(\mathbf{x}_\perp, \mathbf{y}_\perp)$ and $\sigma(\mathbf{x}_\perp)$ discovered in [32] allows rewriting (19) in terms of the real kernel $\chi(\mathbf{x}_\perp, \mathbf{y}_\perp)$ only:

$$\mathcal{H}[\rho] = \frac{1}{2} \int_{\mathbf{x}_\perp, \mathbf{y}_\perp} \frac{\delta}{\delta\rho(\mathbf{x}_\perp)} \, \chi(\mathbf{x}_\perp, \mathbf{y}_\perp) \, \frac{\delta}{\delta\rho(\mathbf{y}_\perp)} \,. \tag{20}$$

The explicit expression for $\chi(\mathbf{x}_\perp, \mathbf{y}_\perp)$ involves the path-ordered exponentials $U(\mathbf{x}_\perp)$ defined in (9):

$$\chi(\mathbf{x}_\perp, \mathbf{y}_\perp) = \int \frac{\mathrm{d}^2 \mathbf{z}_\perp}{4\pi^3} \, \frac{(\mathbf{x}_\perp - \mathbf{z}_\perp)(\mathbf{y}_\perp - \mathbf{z}_\perp)}{(\mathbf{x}_\perp - \mathbf{z}_\perp)^2 (\mathbf{y}_\perp - \mathbf{z}_\perp)^2} \times \Big[\big(1 - U^\dagger(\mathbf{x}_\perp) \, U(\mathbf{z}_\perp)\big) \big(1 - U^\dagger(\mathbf{z}_\perp) \, U(\mathbf{y}_\perp)\big) \Big] \,. \tag{21}$$

Until recently, the use of the JIMWLK evolution equations and their simplified versions, the BK equations [33, 34] corresponding to retaining only the two-point functions in the infinite hierarchy generated by (18), was restricted to one-source problems like deep inelastic scattering at high energies and quantities like gluon structure functions. In a major recent development [35–37], the formalism allowing systematic computation of quantum corrections to the two-source glasma problem for inclusive gluon production was developed. In particular, a generalized factorization property of the two-source problem in high-energy QCD was derived in which both incoming fluxes are described by the solutions of JIMWLK equation (18) characterized by the corresponding saturation scales. This approach allows calculating the inclusive gluon production cross section. Schematically, the leading logarithmic correction to such an observable $\mathcal{O}$ can be written as [35–37]

$$\Delta\mathcal{O} = \left[\log\left(\frac{1}{x_1}\right) \mathcal{H}_1 + \log\left(\frac{1}{x_2}\right) \mathcal{H}_2 \right] \mathcal{O} \,, \tag{22}$$

where $\log(1/x_{1,2})$ are the rapidity shifts taken into account in computing the quantum corrections and $\mathcal{H}_{1,2}$ are the JIMWLK Hamiltonians of the incident nuclei.

3.2 Jet quenching and parton energy loss in a dense non-Abelian medium

As was already mentioned in Section 2, one of the most impressive results of experiments at the RHIC is the dramatic decrease in the yield of particles with large transverse momentum — a phenomenon directly related to the so-called jet quenching in dense QCD matter. The underlying phenomenon is, of course, more general than just the above-mentioned attenuation of the inclusive spectra of transverse momentum, referring rather to specific medium-induced changes in the physics of multiparticle production. The main focus of jet quenching studies is to seek modifications of standard patterns of processes at large transverse momenta (such as jet production in nuclear collisions) compared to the results for pp collisions. The jetty structure of the final state in events characterized by large transverse energies is one of the generic features of particle production in high-energy hadron collisions. The properties of these jets, i.e., the collimated fluxes of hadrons, are very well described, especially in the e^+e^- annihilation, by perturbative QCD under the assumption of the local parton–hadron duality. This refers to both the cross section and the topology of jetty events and the properties of the individual jets, such as intrajet particle distributions and multiplicity distributions. Thus, QCD jet physics is a very natural place to look for medium-induced modifications in nuclear collisions — in the hope that reasonable theoretical and experimental control of its relevant characteristics can be achieved. For recent reviews on theoretical approaches to describing jet quenching and their comparison with experimental data, we refer the reader to [38–45].

Schematically, the process of jet formation can be divided into three stages:

• Production of an initial high-energy parton. At asymptotically high energies, the relevant theoretical description is given by the standard formalism of collinear factorization.

• Creation of a final-state high-energy particle, typically accompanied by radiation. Technically, it is convenient to assign the initially produced parton some virtuality Q_0^2, which is shaken off by subsequent perturbative radiation of gluons and quark–antiquark pairs until reaching some cutoff invariant mass Q_h^2 at which the perturbative description is no longer applicable.

• Hadronization of partonic configuration created in the course of the QCD jet evolution.

For example, we consider the simplest inclusive distribution (fragmentation function) $D^h(x = E_h/E_0, Q_0^2)$ describing the probability of a hadron with the energy $E_h = xE_0$ in a jet originated by a parton[7] with energy E_0 and virtuality Q_0^2. At sufficiently large Q_0^2, we can write

$$D^h(x, Q_0^2) = \int_x^1 dz\, \mathcal{P}(z, Q_h^2, Q_0^2)\, D^h\left(\frac{x}{z}, Q_h^2\right), \qquad (23)$$

where $\mathcal{P}(z, Q_h^2, Q_0^2)$ is the perturbatively calculable probability of producing a parton with the fractional energy $z = E/E_0$ and virtuality Q_h^2 in a jet originated by the parton with energy E_0 and virtuality Q_0^2, and $D^h(E_h/E, Q_h^2)$ is the nonperturbative fragmentation function describing the corresponding parton–hadron conversion. The probabilistic description of the parton–hadron transformation is possible due to the collinear factorization property of QCD, which ensures, at large enough Q_0^2, the absence of interference between the perturbative evolution of the initial parton and the final nonperturbative process of color blanching and formation of the final hadron. The probability $\mathcal{P}(z, Q_h^2, Q_0^2)$ refers to a QCD cascade converting the initial parton into a spray of partons with different fractional energies $\{z\}$ and the same final virtuality Q_h^2. In the in-vacuum QCD, the evolution of the fragmentation function $D_a^h(E_h/E, Q_0^2)$ with Q_0^2 is described by the standard Dokshitzer–Gribov–Lipatov–Altarelli–Parisi (DGLAP) evolution equations [46–48].

At large Q_0^2, the formation of the initial parton occurs at a very small time and, in the first approximation, the medium effects on this initial process can be neglected. But in the in-medium QCD, both the probabilistic kernel $\mathcal{P}(z, Q_h^2, Q_0^2)$ and the nonperturbative fragmentation function $D^h(x = E_h/E, Q_h^2)$ depend, generally speaking, on the properties of the medium. The dominant opinion in the current literature is that all the relevant medium-induced effects take place at the perturbative stage and refer to $\mathcal{P}(z, Q_h^2, Q_0^2)$, leaving $D^h(x = E_h/E, Q_h^2)$ unaffected.[8] Under this assumption, the medium-modified fragmentation function $D_a^{h(med)}(x, Q_0^2)$ can be introduced as

$$D_a^{h(med)}(x, Q_0^2) = \int_x^1 dz \big(\mathcal{P}_{ab}(z, Q_h^2, Q_0^2) + \Delta\mathcal{P}_{ab}(z, Q_h^2, Q_0^2 | \{\mu\})\big)\, D_b^h(x, Q_h^2), \qquad (24)$$

where $\Delta\mathcal{P}_{ab}(z, Q_h^2, Q_0^2 | \{\mu\})$ is the medium-induced change in the in-vacuum probability, which depends on the properties of the medium characterized by the set of parameters $\{\mu\}$.

Calculating $\Delta\mathcal{P}(z, Q_h^2, Q_0^2 | \{\mu\})$ requires understanding the mechanisms of medium-induced effects such as medium-induced radiation and elastic energy loss experienced by a parton propagating in the dense non-Abelian medium. This is discussed in Section 3.2.1.

We note that both of the two medium-induced mechanisms described above are well studied in the Abelian case in the framework of the physics of electromagnetic showers in matter (see, e.g., [49]). An important component of the physics of electromagnetic showers is accounting for ionization losses leading to specific distortions of the pattern resulting from medium-induced bremsstrahlung and pair production [49]. Modifications of QCD cascades with 'pionization,' i.e., the interaction with additional strongly interacting degrees of freedom, taken into account were analytically studied for non-angular-ordered cascades in [50–53] and for angular-ordered ones in [54, 55].

3.2.1 Parton energy loss. We mentioned in the previous paragraph that the process of transformation of the initial highly energetic, highly virtual parton into a spray of the final hadrons is, in some approximations, the process of a perturbative cascading emission of new quanta. Thus, we are dealing, for instance, with the question of multiple gluon emission. To compute generic in-medium corrections to the

[7] In this section, we omit all parton subscripts and consider the purely gluonic cascade for simplicity.

[8] Experimental data that favor it were mentioned in Section 2.

in-vacuum picture, we must, in principle, calculate cross sections for multiple medium-induced gluon emission. To date, this problem has not been solved. At the current level of the theory of medium-induced radiation, the corresponding cross sections for one-gluon emission can be computed in the first order in the strong coupling constant, and, under certain simplifying assumptions, to all orders in the interaction with the medium. The resulting one-gluon emission spectrum can be written as a sum of the vacuum and medium-induced contributions:

$$\frac{\mathrm{d}I^{\mathrm{tot}}}{\mathrm{d}\omega\,\mathrm{d}^2\mathbf{k}_\perp}=\frac{\mathrm{d}I^{\mathrm{vac}}}{\mathrm{d}\omega\,\mathrm{d}^2\mathbf{k}_\perp}+\frac{\mathrm{d}I^{\mathrm{med}}}{\mathrm{d}\omega\,\mathrm{d}^2\mathbf{k}_\perp}\,, \tag{25}$$

where

$$\frac{\mathrm{d}I^{\mathrm{vac}}}{\mathrm{d}\omega\,\mathrm{d}^2\mathbf{k}_\perp}=\frac{\alpha_{\mathrm{s}}}{2\pi}\,\frac{N_{\mathrm{c}}}{\mathbf{k}_\perp^2}\,K^{\mathrm{vac}}(z)\,, \tag{26}$$

and $K^{\mathrm{vac}}(z)=1/[z(1-z)]-2+z(1-z)$ is the standard DGLAP gluonic splitting function. The general case with multiple gluon emission is then considered by constructing a probabilistic branching process obtained by iterating the one-gluon emission described by first-order expression (25). The corresponding theoretical schemes used for constructing such cascades are discussed in Section 3.2.2. Below, we discuss the methods of calculating the second term in the right-hand side of (25) to the accuracy $O(\alpha_{\mathrm{s}})$.

The physical problem under consideration is to compute the leading contribution to the medium-induced energy loss ΔE of a parton produced inside the medium on its way from a hot dense fireball. Generically, the energy loss ΔE depends on the medium thickness L and the bulk characteristics of the medium and is described by some probability distribution $\mathcal{P}(\Delta E)$.

More precisely, the losses are determined by the following factors:

• The probability of an elementary event leading to energy loss characterized by the opacity $N=L/\lambda$, where λ is the mean free path of the parton in the medium. For a particle with the integrated particle–medium interaction cross section σ and medium density ρ, the mean free path can be estimated as $\lambda\sim 1/(\rho\sigma)$.

• The intensity of the impact or scattering power of the medium is characterized by the transport coefficient $\hat{q}=\langle p_\perp^2\rangle/\lambda$, where $\langle p_\perp^2\rangle$ is the average squared transverse momentum acquired by the propagating parton in an elementary act of collision. In the thermal medium, $\hat{q}=m_{\mathrm{D}}^2/\lambda$, where m_{D} is the Debye mass.

There exists a general consensus, supported by extensive model calculations, that the radiative medium-induced energy loss is the dominant one (see, e.g., [56]). Theoretical work on studying the properties of medium-induced gluon radiation was carried out by several groups [57–83]. The approaches of the groups differ in the details of treating the relevant kinematics of the radiation and the details of describing the medium under consideration. In this review, following [40, 43, 44], we sketch the main steps of the approach developed in [67–75]. The two key ideas that allow carrying out the calculation of medium-induced radiation in the form discussed below are the separation of transverse and longitudinal degrees of freedom [84] and the use of the light-cone path integral formalism [72].

We start with the fundamental idea that in QCD, in contrast to QED, the radiation of gluons can be meaningfully considered in the eikonal approximation. This radiation is due to the decoherence of the initial coherent parton flux by soft color rotations caused by the medium fields (see a clear discussion in [40, 44]). The basic objects of the eikonal approximation in QCD are Wilson lines. Staying in the gauge $A^+=0$ used in the previous section, we obtain the following expression for the Wilson line in question:

$$W(\mathbf{x}_\perp)=\mathcal{P}\exp\left[\mathrm{i}g\int \mathrm{d}x^+A^-(x^+,\mathbf{x}_\perp)\right], \tag{27}$$

where $\mathbf{x}_\perp$ is the coordinate of the incident parton in the impact parameter plane, which is constant in the eikonal approximation, and $A^-(x^+,\mathbf{x}_\perp)$ are the target fields. Wilson line (27) fully determines the S-matrix element of eikonal scattering:

$$S(p\to p')\sim\delta(p'^+-p^+)\int \mathrm{d}\mathbf{x}_\perp \times\exp\left[-\mathrm{i}\mathbf{x}_\perp(\mathbf{p}'_\perp-\mathbf{p}_\perp)\right]W(\mathbf{x}_\perp)\,. \tag{28}$$

The cross section is therefore fully specified by the average of the product of Wilson lines taken at different points in the impact parameter plane:

$$\left|S(p\to p')\right|^2\;\to\;\frac{1}{N_{\mathrm{c}}}\left\langle W^\dagger(\mathbf{x}_\perp)\,W(\mathbf{y}_\perp)\right\rangle. \tag{29}$$

To elucidate the physical meaning of the average of the product of Wilson lines in (29), we consider the simplest and at the same time the most popular model of the medium, in which the medium is described as a collection of static field sources $a^-(\mathbf{x}_{\perp i})$ located at points $\{x_i^+\}$ and hence characterized by the density $n(x^+)=\sum_i\delta(x^+-x_i^+)$. For such a medium, the right-hand side of (29) becomes

$$\frac{1}{N_{\mathrm{c}}}\left\langle W^\dagger(\mathbf{x}_\perp)\,W(\mathbf{y}_\perp)\right\rangle\simeq\exp\left\{-\frac{C_R}{2}\int \mathrm{d}x^+n(x^+)\times\sigma(\mathbf{x}_\perp-\mathbf{y}_\perp)\right\}, \tag{30}$$

where $\sigma(\mathbf{x}_\perp-\mathbf{y}_\perp)$ is the cross section of scattering of the color dipole on the target under consideration and C_R is the corresponding Casimir operator:

$$\sigma(\mathbf{x}_\perp-\mathbf{y}_\perp)=\int\frac{\mathrm{d}^2\mathbf{q}_\perp}{(2\pi)^2}\,\mathrm{Tr}\,|a^-(\mathbf{q}_\perp)|^2\times\left\{1-\exp\left[\mathrm{i}(\mathbf{x}_\perp-\mathbf{y}_\perp)\,\mathbf{q}_\perp\right]\right\}. \tag{31}$$

We emphasize that the dipole cross section appears only in the matrix element squared (or, equivalently, the cut diagram); the problem under consideration is that of scattering of a single color probe. In the soft scattering approximation, the dipole scattering cross section is simply expressed as $\sigma(\mathbf{x}_\perp-\mathbf{y}_\perp)\simeq C(\mathbf{x}_\perp-\mathbf{y}_\perp)^2$, and therefore

$$\frac{1}{N_{\mathrm{c}}^2-1}\left\langle W^\dagger(\mathbf{x}_\perp)\,W(\mathbf{y}_\perp)\right\rangle\simeq\exp\left\{\frac{1}{4\sqrt{2}}\int \mathrm{d}x^+\hat{q}(x^+)(\mathbf{x}_\perp-\mathbf{y}_\perp)^2\right\}, \tag{32}$$

where $\hat{q}(\xi)=2\sqrt{2}Cn(\xi)$. Here, $\hat{q}$ is just the above-introduced scattering power of the medium.

To go beyond the soft scattering approximations, the momentum transfer from the medium must be taken into account. The corresponding elegant generalization of (29) is given by

$$S(p\to p')\sim\delta(p'^{+}-p^{+})\,p^{+}\int \mathrm{d}\mathbf{x}_\perp \exp\left[-\mathrm{i}(\mathbf{x}_\perp)(\mathbf{p}'_\perp-\mathbf{p}_\perp)\right]$$
$$\times\int\mathcal{D}\mathbf{r}_\perp(x^{+})\,\exp\left\{\mathrm{i}\,\frac{p^{+}}{2}\int\mathrm{d}x^{+}\left[\frac{\mathrm{d}\mathbf{r}_\perp(x^{+})}{\mathrm{d}x^{+}}\right]\right\}W(\mathbf{r}_\perp)\,. \quad (33)$$

In (33), the momentum transfer from the medium is described by the motion of an effective nonrelativistic particle (a standard situation in the light-cone quantization) in the impact parameter plane.

Formula (33) allows calculating the induced gluon radiation spectrum in the medium of a longitudinal extent L^{+}, with the interference of in-vacuum and in-medium contributions taken into account [67] (see also [75]):

$$k^{+}\frac{\mathrm{d}I}{\mathrm{d}k^{+}\,\mathrm{d}^2\mathbf{k}_\perp}=\frac{\alpha_\mathrm{s}C_R}{\pi^2}\,\frac{1}{\mathbf{k}_\perp^2}+\frac{\alpha_\mathrm{s}C_R}{(2\pi)^2k^{+}}$$
$$\times 2\mathrm{Re}\int_{x_0^{+}}^{L^{+}}\mathrm{d}x_1^{+}\int\mathrm{d}^2\mathbf{x}_\perp\exp\left(-\mathrm{i}\mathbf{k}_\perp\mathbf{x}_\perp\right)$$
$$\times\left[\frac{1}{k^{+}}\int_{x_2^{+}}^{L^{+}}\mathrm{d}x_2^{+}\,\exp\left(-\frac{1}{2}\int_{x^{+}}^{L^{+}}\mathrm{d}\xi n(\xi)\,\sigma(\mathbf{x}_\perp)\right)\right.$$
$$\times\frac{\partial}{\partial\mathbf{y}_\perp}\,\frac{\partial}{\partial\mathbf{x}_\perp}\,\mathcal{K}(\mathbf{x}_\perp,x_2^{+}|\,\mathbf{0},x_1^{+})$$
$$\left.-\,2\,\frac{\mathbf{k}_\perp}{\mathbf{k}_\perp^2}\,\frac{\partial}{\partial\mathbf{y}_\perp}\mathcal{K}\big(\mathbf{x}_\perp,L^{+}|\,\mathbf{0},x_1^{+}\big)\right]. \quad (34)$$

Here, $\mathcal{K}(\mathbf{r}_\perp(x_2^{+})|\mathbf{r}_\perp(x_1^{+}))$ is the Green's function

$$\mathcal{K}\big(\mathbf{r}_\perp(x_2^{+})|\,\mathbf{r}_\perp(x_1^{+})\big)$$
$$=\int\mathcal{D}\mathbf{r}_\perp\exp\left\{\int_{x_1^{+}}^{x_2^{+}}\mathrm{d}\xi\left(\mathrm{i}\,\frac{p^{+}}{2}\,\dot{\mathbf{r}}_\perp^2-\frac{1}{2}\,n(\xi)\,\sigma(\mathbf{r}_\perp)\right)\right\}. \quad (35)$$

In the soft scattering approximation, Green's function (35) is simplified to

$$\mathcal{K}\big(\mathbf{r}_\perp(x_2^{+})|\,\mathbf{r}_\perp(x_1^{+})\big)$$
$$=\int\mathcal{D}\mathbf{r}_\perp\exp\left\{\mathrm{i}\,\frac{p^{+}}{2}\int_{x_1^{+}}^{x_2^{+}}\mathrm{d}\xi\left(\dot{\mathbf{r}}_\perp^2+\mathrm{i}\,\frac{\hat{q}(\xi)}{2\sqrt{2}p^{+}}\,\mathbf{r}_\perp^2\right)\right\}. \quad (36)$$

The expansion in opacity or, equivalently, in the density of the medium is obtained by expanding (34) in the cross-section σ.

The physics behind the full expression (34) can be illustrated by considering a soft gluon emission. The formation time of a gluon is $\tau_\mathrm{form}\sim 2\omega/k_\perp^2$. This time should be long enough to ensure the phase change $\Delta\Phi\sim 1$ sufficient for decoherence and hence radiation. In more detail,

$$\Delta\Phi=\left\langle\frac{L}{\tau_\mathrm{form}}\right\rangle\sim\left\langle\frac{k_\perp^2}{2\omega}\,\Delta z\right\rangle=\frac{\hat{q}L}{2\omega}\,L\equiv\frac{\omega_\mathrm{c}}{\omega}\,, \quad (37)$$

where

$$\omega_\mathrm{c}=\frac{1}{2}\,\hat{q}L^2\,. \quad (38)$$

In the limit $\omega\ll\omega_\mathrm{c}$, the medium acts coherently, reducing the intensity of radiation, while the limit $\omega\gg\omega_\mathrm{c}$ corresponds to incoherent scattering:

$$\omega\,\frac{\mathrm{d}I}{\mathrm{d}\omega}\bigg|_{\omega\ll\omega_\mathrm{c}}\approx\alpha_\mathrm{s}\sqrt{\frac{\hat{q}L^2}{\omega}}\,,$$
$$\omega\,\frac{\mathrm{d}I}{\mathrm{d}\omega}\bigg|_{\omega\gg\omega_c}\approx\alpha_\mathrm{s}\,\frac{\hat{q}L^2}{\omega}\,. \quad (39)$$

In the soft limit $\omega\ll\omega_\mathrm{c}$, the average energy loss is

$$\langle\Delta E\rangle\simeq\int_0^{\omega_\mathrm{c}}\mathrm{d}\omega\,\omega\,\frac{\mathrm{d}I}{\mathrm{d}\omega}\sim\hat{q}L^2\,. \quad (40)$$

For some time, it was believed that the quadratic dependence on the medium thickness L is a specifically non-Abelian effect. Recently, however, it was shown in [85] (see also [86]) that the effect is generic and is valid in both QED and QCD for the radiation of a particle produced inside the medium in the initial part of its trajectory.

3.2.2 Multiple gluon emission. In-medium QCD cascades. We begin with the simplest version of taking the multiple medium-induced gluon emission into account, with the evolution of the timelike QCD shower in virtuality neglected. Here, the possibility of multiple emission is taken into account by constructing a simple Poissonian picture in which the probability distribution of the cumulative energy loss $\mathcal{P}(\Delta E)$ is given by

$$\mathcal{P}(\Delta E)=p_0\sum_{n=0}^{\infty}\frac{1}{n!}\int\left[\prod_{i=1}^{n}\mathrm{d}\omega_i\int\mathrm{d}\omega_i\,\mathrm{d}k_{\perp i}\,\frac{\mathrm{d}I^\mathrm{med}}{\mathrm{d}\omega_i\,\mathrm{d}k_{\perp i}}\right]$$
$$\times\,\delta\left(\sum_{i=1}^{n}w_i-E\right),$$
$$p_0=\exp\left[-\int\mathrm{d}\omega\,\mathrm{d}k_\perp\,\frac{\mathrm{d}I^\mathrm{med}}{\mathrm{d}\omega\,\mathrm{d}k_\perp}\right]. \quad (41)$$

The Poissonian cascade described by (41) can be derived from the full DGLAP evolution (see the appendix in [7]). Knowing $\mathcal{P}(\Delta E)$ allows computing the distribution $\mathcal{P}(\varepsilon)$ of the fractional energy loss $\varepsilon=\Delta E/E_0$ of a parton with the initial energy E_0 and obtaining the equation for the medium-modified fragmentation function originally suggested in [88]:

$$\mathcal{D}_{a\to\mathrm{h}}^{m}(z,Q^2)=\int\frac{\mathrm{d}\varepsilon}{1-\varepsilon}\,\mathcal{P}(\varepsilon)\,\mathcal{D}_{a\to\mathrm{h}}\left(\frac{z}{1-\varepsilon},\,Q^2\right). \quad (42)$$

Next, turning to the discussion of the complete picture, we stress once again that the energy flow in the in-vacuum high-energy processes involving quarks and gluons that are characterized by large momentum transfer is dominated by well-collimated jets originating from multiple cascading radiation of gluons and quark–antiquark pairs. The physical origin of the cascading process is the intense gluon radiation of a high-energy parton created in a hard subprocess. From the operational standpoint, this radiation can be regarded as a cascade degradation of the (large) virtuality of the initial parton until reaching some nonperturbative scale Q_h at which preconfined colorless clusters and/or QCD strings are formed.

For detailed studies of in-vacuum QCD cascades, Monte Carlo simulations are used. The two most popular versions of

these MC generators are PYTHIA [89] and HERWIG (Hadron Emission Reactions With Interfering Gluons) [90–92]. Both of them implement the key feature of in-vacuum QCD cascades, the angular ordering of successive decays that has its origin in fine-tuned quantum coherence effects. In the older version of PYTHIA, the angular-ordering restrictions were implemented by hand, while in its later versions and in HERWIG, they are accounted for by a construction owing to the choice of an appropriate evolution variable. In the presence of the medium, new mechanisms appear that change the structure of in-vacuum QCD jets. In an in-vacuum cascade, the only source of evolution is the initial virtuality of the jet. In the in-medium case, the medium acts as a source of 'extra' virtuality for the propagating partons, resulting in induced radiation and a sink of energy due to the energy loss resulting from elastic and inelastic collisions of propagating partons with the particles in the medium. The first MC code adding medium-induced radiation was PYQUEN (Pythia QUENched) [93]. Recently, MC codes have appeared describing the medium-induced effects in QCD cascades such as JEWEL [94], Q-PYTHIA [95] (both based on the mass-ordered version of PYTHIA), and Q-HERWIG [96] based on HERWIG.

We reiterate that the complete picture combining the in-vacuum and in-medium evolution is still not available. The main difficulty lies in the fact that the medium created in high-energy nuclear collisions is necessarily finite, and hence modifications induced by the medium are dependent on its characteristics in space–time: the cascade must be placed inside the medium: in Fig. 1, the origin of the cascade is placed at some distance L from the border separating the dense medium from the normal vacuum.

Obviously, the larger the distance of parton propagation in the medium is, the bigger the medium-induced losses. In describing the in-medium QCD cascade, the key question is therefore how to choose the language allowing a credible space–time interpretation. As emphasized in [94], the only scheme allowing such an interpretation is the old-style PYTHIA virtuality-ordered cascade, where connection to the space–time pattern is achieved by calculating the lifetime τ of a virtual parton; for a parton with energy E and virtuality Q^2 that has been created in the decay of its parent parton with virtuality $Q^2_{\rm par}$, the lifetime is given by

$$\tau = E\left(\frac{1}{Q^2}-\frac{1}{Q^2_{\rm par}}\right). \tag{43}$$

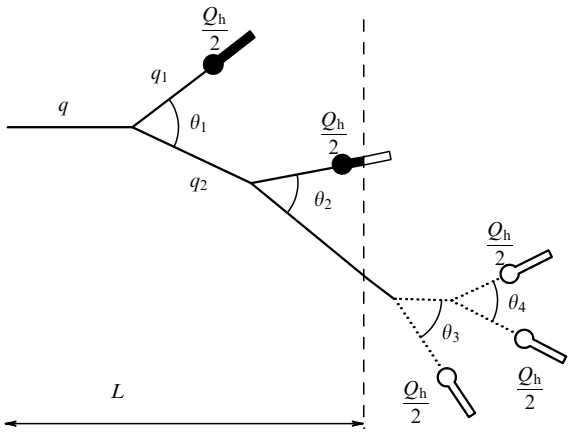

Figure 1. QCD cascade in a medium.

The lifetime of the initial parton is taken to be $\tau_{\rm in} = E_{\rm in}/Q^2_{\rm in}$. For example, the time $\tau_{\rm h}$ at which the parton with the momentum q_1 in Fig. 1 produced the final prehadron is

$$\tau_{\rm h} = E_0\,\frac{1}{Q_0^2} + E_1\left(\frac{4}{Q_{\rm h}^2}-\frac{1}{Q_0^2}\right) = \frac{E_0}{Q_0^2}\left[1+x\left(\frac{4Q_0^2}{Q_{\rm h}^2}-1\right)\right],$$

where $x = E_1/E_0$. We have already mentioned that in the overwhelming majority of studies devoted to energy loss in high-energy nuclear collisions, it is assumed that hadronization occurs outside the hot and dense fireball. Setting up a temporary scale using formula (43) helps address this issue quantitatively [97]. For example, for the parton q_1 in Fig. 1, it happened that $\tau_{\rm h} < L$, and hence both its formation at time E_0/Q_0^2 and its decay into the final prehadron occurred inside the medium. To give an idea of the underlying physics, we consider, for example, a gluon with the energy $E_0 = 100$ GeV equipped with a typical initial invariant mass $Q_0 = 10$ GeV. On average, this gluon decays at $\tau_0 \sim E_0/Q_0^2 = 1\ \text{GeV}^{-1} \simeq 0.2$ fm, and hence, if the vertex in which the initial hard gluon was generated was sufficiently far (several fermis) from the surface of a hot fireball, then a significant part of the cascade vertices would in fact be generated inside the medium.

In what follows, we concentrate on the description of the old-style PYTHIA virtuality-ordered cascade and its in-medium modifications. The cascade evolution goes through a sequence of decays $q \Rightarrow q_1 + q_2$, where $q = (E, \mathbf{q})$ is a four-momentum of the parent gluon and q_1 and q_2 are those of the daughter ones. We study the timelike evolution in which cascading reshuffles the initial jet virtuality such that $q^2 > q_1^2 + q_2^2$ at each decay. The cascading process at a given branch stops when the virtuality of the last parton reaches a threshold level $Q_{\rm h}^2$, i.e., no decay into two partons with the minimal virtuality $Q_{\rm h}^2/4$ can occur. The key property of the in-vacuum QCD cascades, the effective angular ordering of subsequent decays due to color coherence (for example, ensuring that $\theta_2 < \theta_1$ in Fig. 1), is not automatically taken into account in the mass-ordered evolution and has to be enforced explicitly by accepting only those generated decays for which the condition of angular ordering does hold. The basic component of the probabilistic formalism of the QCD cascade evolution is the conditional probability of a parton produced at the scale $Q^2_{\rm in}$ with an energy E undergoing a subsequent decay at the scale $Q^2 < Q^2_{\rm in}$ into two daughter partons with energies zE and $(1-z)E$; this probability can be calculated from the Sudakov formfactor

$$S\left(Q^2|\,E, Q^2_{\rm in}; Q^2_{\rm h}\right) = \exp\left[-\int_{Q^2}^{Q^2_{\rm in}} {\rm d}\mathbf{k}_\perp^2 \int_{z_-(E,\,\mathbf{k}_\perp^2|\,Q^2_{\rm h})}^{z_+(E,\,\mathbf{k}_\perp^2|\,Q^2_{\rm h})} {\rm d}z\,\frac{{\rm d}I^{\rm tot}}{{\rm d}z\,{\rm d}^2\mathbf{k}_\perp}\left(\mathbf{k}_\perp^2, z\right)\right], \tag{44}$$

where $z_\pm(E,\ k_\perp^2|\ Q_{\rm h}^2)$ define the kinematic limits available for the parton decay,

$$z_\pm\left(E, Q^2|\ Q^2_{\rm h}\right) = \frac{1}{2}\left(1 \pm \sqrt{\left(1-\frac{Q^2}{E^2}\right)\left(1-\frac{Q^2_{\rm h}}{Q^2}\right)}\right), \tag{45}$$

and where the full differential probability of gluon emission ${\rm d}I^{\rm tot}/{\rm d}z\,{\rm d}^2\mathbf{k}_\perp$ was defined in (25).

When considering the properties of in-medium QCD cascades, we have to deal with several mechanisms modifying the in-vacuum intrajet characteristics, in particular, the loss of quantum coherence and the resulting disruption of the

angular ordering for decays inside the medium, the medium-induced radiation (inelastic energy loss), and the elastic scattering of partons on particles in the medium (elastic energy loss). Below, we describe the corresponding modifications to the MC procedure for the generation of those in-vacuum QCD cascades that take these features into account.

We start with the decoherence-induced disruption of angular ordering [97]. The violent environment created in ultrarelativistic heavy ion collisions acts as a source of random energy–momentum and color with respect to the diagrams for the in-vacuum processes. Generally speaking, this kind of random impact destroys the phase tuning lying at the heart of quantum interference phenomena. Those situations in which random external influences destroy interference-related effects are very common in solid state physics. A well-studied example is provided by the destruction of weak localization in the presence of random external impacts (see, e.g., [98, 99]). Therefore, it is intuitively quite clear that the quantum coherence effects should be broken in the violent environment created in heavy ion collisions. This was first explicitly mentioned in [94], in which the origin of decoherence and the ensuing disappearance of angular ordering was related to the rescattering of cascading particles on scattering centers in the medium. Another argument in support of the assumption of angular decoherence is that at least at the Vlasov approximation level, the characteristic time of color randomization is much less than the characteristic scattering time [100, 101]. Because color randomization alone is sufficient for angular decoherence, one could expect that this effect is even stronger than assumed in [94]. The simplest assumption taking this effect into account is that the angular ordering is broken for all decays that occur inside the medium. The effect is thus directly dependent on the size of the medium available for cascade development. In terms the notation introduced in Fig. 1, the effect is L-dependent. The corresponding modifications of the rapidity distributions are shown in Fig. 2. We see that the decoherence effects alone, i.e., before considering the medium-induced energy loss, lead to substantial softening of the intrajet particle spectrum.

It is important to note that, as seen from Fig. 2, the softening of the intrajet rapidity distribution sets in at relatively small medium sizes $L \sim 1$ fm.

We now turn to the effects of the medium-induced radiation. A rigorous treatment of this problem is very difficult. Only very recently was an elegant formalism that allows taking LPM effects into account in the MC cascades described in [102, 103].

The results of modifications of the QCD cascade properties were obtained using simpler schemes based on various approximations for the effective differential spectrum (25) or, equivalently, the modified splitting function

$$K^{\mathrm{tot}}(z, E, Q^2, \hat{q}, L) = K^{\mathrm{vac}}(z) + \Delta K(z, E, Q^2, \hat{q}, L)\,, \quad (46)$$

which depends, generally speaking, not only on the energy ratio z but also on the energy and virtuality of the parent parton, the stopping power of the medium, the path length in the medium, and so on [104].

The simplest version of the medium-modified splitting function mimicking the effects of medium-induced radiation was suggested in [105]:

$$K_{\mathrm{vac}}(z) \to (1 + f_{\mathrm{med}})\, K_{\mathrm{vac}}(z)\,. \quad (47)$$

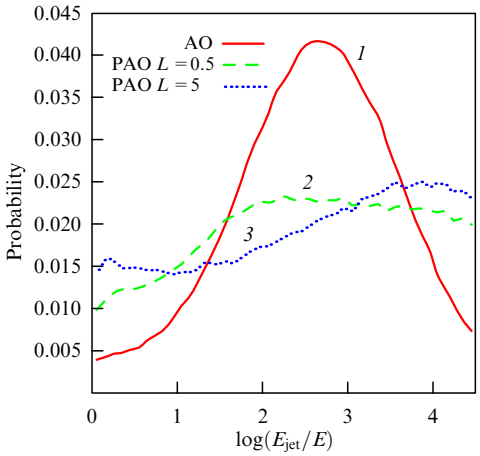

Figure 2. Distribution in the rapidity $P(y)$ of final prehadrons: *1*, $L = 0$, full angular ordering, solid red line; *2*, $L = 0.5$ fm, partial angular ordering, dashed green line; *3*, $L = 5$ fm, partial angular ordering, dotted blue line [97].

A more advanced definition of the medium-induced splitting function was proposed in [87]:

$$\Delta K(z, E, Q^2, \hat{q}, L) \simeq \frac{2\pi Q^2}{\alpha_{\mathrm{s}}} \frac{\mathrm{d}I^{\mathrm{med}}}{\mathrm{d}z\,\mathrm{d}Q^2}\,, \quad (48)$$

where $\mathrm{d}I^{\mathrm{med}}/\mathrm{d}z\,\mathrm{d}Q^2$ is taken from Eqn (34).

With the concrete expressions for the modified splitting functions like (47) and (48), the main component for describing the cascade, Sudakov formfactor (44), is fully specified.

The main quantity addressed in these MC simulations is the jet quenching ratio $R_{\mathrm{AA}}(p_\perp)$. Agreement with the experimental data is achieved by tuning the parameters of the medium like $\hat{q}^2$ or f^{med}. In most cases, agreement can indeed be reached, albeit at the expense of very large variations in the values of these parameters obtained within different formalisms and of the numerous theoretical uncertainties.

As regards more generic intrajet characteristics, the general expectations concerning the effect of the medium-induced interactions are:

- Softening of the rapidity distributions.
- Broadening of the distributions in transverse momentum.
- Increased multiplicity.

These expectations are indeed confirmed by the studies undertaken with the above-described MC generators [94, 95] (see also [106]). More involved properties of medium-modified cascades, such as higher-order multiplicity moments, have also been studied in the literature [107, 108].

4. Macroscopic approach to the quark–gluon medium

The macroscopic collective properties of a medium may be revealed in its mechanical motion as a whole (e.g., viscosity) described by hydrodynamics or in its response to external color currents (e.g., chromopermittivity) described by in-medium QCD. Here, we are mostly dealing with the latter approach, discussing hydrodynamics very briefly at the end because many extensive reviews of it exist (see, e.g., [109, 110]).

Considering the evolution of energy flows due to elastic scattering, bremsstrahlung, or synchrotron radiation, we follow the fate of an initial source (a particle, a parton, a dipole, etc.) and the medium impact on these processes. The evolution of its velocity vector is crucial for conclusions about its energy losses. The notion of the coherence length becomes important when multiple rescattering is taken into account.

However, the medium itself can radiate in response to permutations. The genuine role of the medium and its collective properties are most clearly revealed by its polarization **P** due to an external current. The macroscopic approach to the description of such collective properties is the most suitable one. The linear response of the medium to the electromagnetic field **E** is usually described as

$$\mathbf{P} = \frac{\epsilon - 1}{4\pi}\,\mathbf{E}\,, \tag{49}$$

where ϵ is the dielectric permittivity. It follows that the polarization can be quite strong for large values of ϵ. The initial radiation process serves as a trigger for the collective response of the medium initiated by the polarization. Well-known examples are provided by Cherenkov radiation, the wake, and transition radiation. Typical for their description is the (approximate) constancy of the particle velocity vector used in the external current. In ultrarelativistic processes ($\gamma \gg 1$), the relative change in the velocity is much smaller than the relative energy loss because they are related by the formula

$$\frac{\Delta E}{E} = (\gamma^2 - 1)\,\frac{\Delta v}{v}\,, \tag{50}$$

and the above statement is well supported. The velocity loss can become noticeable only for nonrelativistic partons.

In what follows, we consider very high energy processes. It is well known that gluons become the main component of the wave functions of colliding hadrons. At the LHC, the gg-luminosity is at least an order of magnitude higher than the $\sum$qq-luminosity. Therefore, the in-medium gluodynamics [111] is considered below, simplifying the formulas. Quarks can also be included without difficulty [112].

4.1 Equations of the in-medium QCD

The in-medium equations of gluodynamics differ from the in-vacuum equations by taking the chromopermittivity of the quark–gluon medium into account. Similarly to the dielectric permittivity in electrodynamics, it describes a linear response of matter to passing partons. At the leading order in the coupling constant, the equations are completely analogous to electrodynamic ones, with the chromopermittivity just replacing the dielectric permittivity.

The classical in-vacuum Yang–Mills equations are

$$D_\mu F^{\mu\nu} = J^\nu\,, \tag{51}$$

$$F^{\mu\nu} = \partial^\mu A^\nu - \partial^\nu A^\mu - \mathrm{i}g[A^\mu, A^\nu]\,, \tag{52}$$

where $A^\mu = A^\mu_a T_a$, $A_a(A^0_a \equiv \Phi_a, \mathbf{A}_a)$ are the gauge field (scalar and vector) potentials, the color matrices T_a satisfy the relations $[T_a, T_b] = \mathrm{i}f_{abc}T_c$, $D_\mu = \partial_\mu - \mathrm{i}g[A_\mu, \cdot]$, $J^\nu(\rho, \mathbf{j})$ is a classical source current, and the metric tensor is $g^{\mu\nu} = \mathrm{diag}(+,-,-,-)$.

In the covariant gauge $\partial_\mu A^\mu = 0$, the equations are written as

$$\Box A^\mu = J^\mu + \mathrm{i}g[A_\nu, \partial^\nu A^\mu + F^{\mu\nu}]\,, \tag{53}$$

where $\Box$ is the d'Alembertian operator. The leading term in the expansion in the coupling constant for the classical gluon field is therefore given by a solution of the corresponding Abelian problem.

The chromoelectric and chromomagnetic fields are

$$E^\mu = F^{\mu 0}\,, \tag{54}$$

$$B^\mu = -\frac{1}{2}\,\epsilon^{\mu ij}F^{ij}\,, \tag{55}$$

or, as functions of gauge potentials in vector notation,

$$\mathbf{E}_a = -\mathrm{grad}\,\Phi_a - \frac{\partial \mathbf{A}_a}{\partial t} + g f_{abc}\mathbf{A}_b\Phi_c\,, \tag{56}$$

$$\mathbf{B}_a = \mathrm{rot}\,\mathbf{A}_a - \frac{1}{2}\,g f_{abc}[\mathbf{A}_b\mathbf{A}_c]\,. \tag{57}$$

Equations of motion (51) in vector form are written as

$$\mathrm{div}\;\mathbf{E}_a - g f_{abc}\mathbf{A}_b\mathbf{E}_c = \rho_a\,, \tag{58}$$

$$\mathrm{rot}\,\mathbf{B}_a - \frac{\partial \mathbf{E}_a}{\partial t} - g f_{abc}\bigl(\Phi_b\mathbf{E}_c + [\mathbf{A}_b\mathbf{B}_c]\bigr) = \mathbf{j}_a\,. \tag{59}$$

The effects due to the medium are accounted for if ρ_a and $\mathbf{j}_a$ contain both external and internal (induced) terms. However, similarly to electrodynamics, the role of internal currents can be represented in the linear response approach by the medium permittivity ϵ if **E** is replaced with $\mathbf{D} = \epsilon\mathbf{E}$ in $F^{\mu\nu}$, e.g., in Eqn (54). After that is done, only external currents should be considered in the right-hand sides of the equations. Therefore, Eqns (58) and (59) in vector form are most suitable for generalization to the in-medium case.

In terms of potentials, the equations of *in-medium* gluodynamics are written in the form [111]

$$\begin{aligned}\triangle\mathbf{A}_a - \epsilon\frac{\partial^2\mathbf{A}_a}{\partial t^2} = -\mathbf{j}_a - g f_{abc}\Bigg(&\frac{1}{2}\,\mathrm{rot}\,[\mathbf{A}_b, \mathbf{A}_c]\\ &+ \epsilon\,\frac{\partial}{\partial t}\,(\mathbf{A}_b\Phi_c) + \frac{1}{2}\,[\mathbf{A}_b\,\mathrm{rot}\,\mathbf{A}_c]\\ &- \epsilon\Phi_b\,\frac{\partial \mathbf{A}_c}{\partial t} - \epsilon\Phi_b\,\mathrm{grad}\,\Phi_c - \frac{1}{2}\,g f_{cmn}\bigl[\mathbf{A}_b[\mathbf{A}_m\mathbf{A}_n]\bigr]\\ &+ g\epsilon f_{cmn}\Phi_b\mathbf{A}_m\Phi_n\Bigg),\end{aligned} \tag{60}$$

$$\begin{aligned}\triangle\Phi_a - \epsilon\,\frac{\partial^2\Phi_a}{\partial t^2} = &-\frac{\rho_a}{\epsilon} + g f_{abc}\\ &\times\left(-2\mathbf{A}_c\,\mathrm{grad}\,\Phi_b + \mathbf{A}_b\,\frac{\partial \mathbf{A}_c}{\partial t} - \epsilon\,\frac{\partial\Phi_b}{\partial t}\,\Phi_c\right)\\ &+ g^2 f_{amn}f_{nlb}\mathbf{A}_m\mathbf{A}_l\Phi_b\,.\end{aligned} \tag{61}$$

If the terms explicitly involving the charge g are neglected, we obtain a set of Abelian equations, which differ from electrodynamic equations by the color index a only. The most important property of these equations is that, while the in-vacuum ($\epsilon = 1$) equations do not admit any radiation processes, solutions for $\epsilon \neq 1$ appear with a nonzero Poynting vector even in the classical approach. They predict coherent effects such as Cherenkov gluons, the wake, and transition radiations (see Section 4.3). This corresponds well to the microscopic description in which the matter, at early times after a heavy ion collision, is described in terms of a coherent classical field.

As noted above, $\mathbf{j}_a$ is now treated as an external current assigned to partons moving fast relative to the other partons 'at rest.' It is proportional to g, as seen from Eqn (67) below. The potentials are also of the order of g if the g-dependence of ϵ discussed in Section 4.2 is neglected. Hence, the terms explicitly involving g in the right-hand sides of Eqns (60) and (61) would be of the order g^3. The higher-order corrections may be calculated (see Section 4.5) and a quite interesting conclusion about the color rainbow is obtained.

4.2 Chromopermittivity

The most economical way to describe the matter properties is to take the impact of internal currents in the medium into account phenomenologically by the chromopermittivity ϵ introduced as a constant in Eqns (60) and (61). Its space–time dependence may be included, similarly to electrodynamics. For the Fourier components of ϵ, this would imply a dependence on the frequency ω and the wave vector $\mathbf{k}$. It is well known in electrodynamics that the magnetic permeability is then automatically taken into account. Therefore, it is necessary to consider the permittivity tensor and its color dependence.

These complications can become important, but they are often ignored even in electrodynamics. The medium is often assumed to be isotropic and homogeneous. Methods of linear response theory are used. The ω-dependence is commonly accounted for because the dielectric permittivity of ordinary substances depends on ω. Moreover, it has an imaginary part determining the absorption. The energy behavior of ϵ determines the scales specific to a particular substance.

All these features are typically found experimentally using the relation

$$\epsilon = n^2 \tag{62}$$

between the dielectric permittivity and the refractive index n. For example, both $\mathrm{Re}\,\epsilon$ and $\mathrm{Im}\,\epsilon$ for water have been measured in a wide energy interval ranging over 20 orders of magnitude [113]. The real part $\mathrm{Re}\,\epsilon$ is approximately constant in the visible light region ($\sqrt{\epsilon} \approx 1.34$), increases at low ω (up to $\epsilon \approx 80$), and becomes less than 1 at high energies, tending to 1 at frequencies exceeding the Langmuir (plasma) frequency ω_{L} as

$$\mathrm{Re}\,\epsilon = 1 - \frac{\omega_{\mathrm{L}}^2}{\omega^2}\,. \tag{63}$$

The imaginary part ($\mathrm{Im}\,\epsilon$) responsible for the absorption is very small for visible light, but drastically increases in nearby regions at both low and high frequencies (in this way Nature saves our eyes!).

Therefore, there exist at least two characteristic scales for $\mathrm{Re}\,\epsilon$: just below the optical region and the high-energy scale determined by the Langmuir frequency related to the proper plasma oscillations. The borders of the optical region define the scales for $\mathrm{Im}\,\epsilon$. Theoretically, this behavior is ascribed to various collective excitations in water relevant to its response to radiation with different frequencies. Among them, resonance excitations are quite prominent (see, e.g., [114]). Even in electrodynamics, a quantitative theory of this behavior is still lacking, however. Moreover, formula (63) is a purely electrodynamic one and does not account for hadronic processes at extremely high energies, where the hadronic components of photon wave functions are important.

What can we say then about the chromopermittivity?

The chromopermittivity can be calculated from the polarization operator. Up to now, attempts to calculate the chromopermittivity from first principles have not been very convincing. The corresponding dispersion branches have been computed in the lowest-order perturbation theory [115–118]. The properties of collective excitations have been studied in the framework of thermal field theories [119–123]. In these studies, the simplest perturbative results representing ϵ are generalized by summing some types of diagrams. Only time-like dispersion relations were obtained in this way. A space-like dispersion relation was obtained in [124] in the framework of the method using an *ad hoc* assumption about a special role of scalar resonances. Some studies were performed in [112]. All of these studies refer to a weakly coupled medium. The phenomenological model built upon some intuitive guesses (see, e.g., [125]) was also studied. The physical consequences of introducing chromopermittivity could be mimicked in a microscopic approach by considering different nonzero masses and coupling constants of in-vacuum and in-medium gluons (see, e.g., [72–74, 126–130]), which would allow varying the dispersion relations. However, no convincing principles for choosing them exist, and the number of adjustable energy-dependent parameters increases, even though they are related to more fundamental microscopic notions.

Experimental data certainly favor a strong response of the medium to the deposited energy. This implies that the chromopermittivity must be defined in terms of nonperturbative in-medium gluon field correlation functions, which are currently unknown. Therefore, it makes sense to consider the chromopermittivity as a complicated function of g and, correspondingly, Eqns (60) and (61) as strongly nonlinear in g, even at the classical level, because $\epsilon \neq 1$ takes some quantum and non-Abelian effects into account.

In view of this situation, we prefer to use the general formulas of scattering theory [113, 131] to estimate the chromopermittivity. It can be expressed [113, 131, 132] through the real part of the forward scattering amplitude $\mathrm{Re}\,F_0(\omega)$ for the corresponding quantum[9]

$$\mathrm{Re}\,\Delta\epsilon = \mathrm{Re}\,\epsilon(\omega) - 1 = \frac{4\pi N_{\mathrm{s}}\,\mathrm{Re}\,F_0(\omega)}{\omega^2} = \frac{N_{\mathrm{s}}\sigma(\omega)\rho(\omega)}{\omega}\,, \tag{64}$$

with

$$\mathrm{Im}\,F_0(\omega) = \frac{\omega}{4\pi}\,\sigma(\omega)\,. \tag{65}$$

Here, ω denotes the energy, N_{s} is the density of scattering centers, $\sigma(\omega)$ is the cross section, and $\rho(\omega)$ is the ratio of real and imaginary parts of the forward scattering amplitude $F_0(\omega)$. The sign of $\Delta\epsilon$ coincides with the sign of $\rho(\omega)$.

Unfortunately, we are unable to calculate these characteristics of gluons directly in QCD and have to rely on analogies and our knowledge of the properties of hadron interactions. The experimental facts collected for this medium are brought about only by particles registered at the final stage. We hope that some of their features are also relevant for gluons as the carriers of strong interactions. Those are the resonant behavior of amplitudes at rather low energies and the

[9] In electrodynamics, these quanta are photons, and in QCD, they are gluons.

positive real part of the forward scattering amplitudes at very high energies for hadron–hadron (pp, Kp, πp) and photon–hadron (γp) processes measured from the interference of the Coulomb and hadronic parts of the amplitudes. The last feature is directly connected with the specific property of hadronic processes, the energy increase of the total cross sections, by the dispersion relations for forward scattering amplitudes.

Any Breit–Wigner amplitude has a positive (negative) real part below (above) its peak. The combined effect of all collective resonance excitations in the medium may lead to positive $\Delta\epsilon$ in a wide energy interval at low energies. This is a necessary condition for Cherenkov effects. As explained in Section 4.3.1, the double-humped events at the RHIC and the asymmetry of mass shapes of resonances passing through the quark–gluon medium observed at the SPS may be explained in this way.

At very high energies above the threshold $\omega_{\rm th}$ of the positiveness of real parts of the amplitudes in (64), we can try to use a simple model with

$$\mathrm{Re}\,\epsilon = \left(1+\frac{\omega_0^2}{\omega^2}\right)\Theta(\omega-\omega_{\rm th})\,. \tag{66}$$

Model (66) satisfies the Kramers–Kronig requirement for $\mathrm{Re}\,\epsilon$ to be an even function and approaches 1 at infinity. If experimental data on $\mathrm{Re}\,\epsilon$ for hadrons are inserted into Eqn (64), a form for $\mathrm{Re}\,\epsilon$ follows that is very close to Eqn (66) (see Fig. 1 in [133, 134]). Cosmic ray events with a ringlike (conical) structure may then be explained.

At intermediate energies between these two intervals, similar arguments would favor negative values of $\Delta\epsilon$. Hence, no Cherenkov gluons would be emitted with such energies. The gluon transition radiation (Section 4.3.3) is not forbidden, however. The wake effects (Section 4.3.2) can be shown to be small (see Section 4.3.2).

It is tempting to conclude that energy scales determining the behavior of the real part of the chromopermittivity are not directly related either to the temperature T or to the QCD scale $\Lambda_{\rm QCD}$ of the order of hundreds of MeV but extend to higher values defined by the end of the resonance region (about several GeV) and by the threshold value $\omega_{\rm th}$ connected with an energy increase of the hadronic total cross sections (about tens of GeV). The microscopic nature of their origin is still unclear.

There is another important problem with the definition of chromopermittivity: in-medium equations (60) and (61) are not Lorentz covariant. In macroscopic electrodynamics, the rest frame of matter is well defined and the dielectric permittivity is considered only there. For collisions of two nuclei (or hadrons), the definition of ϵ depends on the geometry of the experiment. Therefore, a Lorentz-covariant chromopermittivity tensor must be considered. The spectra of classical Cherenkov radiation in moving media were calculated in [135] and with quantum corrections, in [136].

The notions of dilute and dense systems [i.e., the value of $N_{\rm s}$ in (64)] depend on values of x and $p_{\rm T}$ at which the wave functions of colliding nuclei are probed. Due to Lorentz transformations, partons moving in different directions with different energies can 'feel' different states of matter in the *same* collision of two nuclei because of the dispersive dependence of the chromopermittivity. We discuss this when dealing with different experimental data and with the problem of instabilities of the quark–gluon medium (Section 4.4).

4.3 Classical polarization effects in the quark–gluon medium and its chromodynamic properties

In view of the similarity between classical QCD and QED equations it would be no surprise to observe some effects in nucleus collisions reminiscent of those in electrodynamics. Actually, this idea was first promoted in [133, 134] relying on the similarity of quarks to electrons and gluons to photons. The emission of Cherenkov gluons, analogous to Cherenkov photons, was predicted and used for the interpretation of a cosmic ray event just observed [137]. These events are discussed in Section 4.3.1.B. This idea received strong support much later, however, from the RHIC data on nucleus–nucleus collisions (see Section 4.3.1.A).

Before delving into experimental data, we describe classical solutions of Eqns (60) and (61). As usual, the current with a constant velocity $\mathbf{v}$ along the z axis is considered:

$$\mathbf{j}(\mathbf{r},t) = \mathbf{v}\rho(\mathbf{r},t) = 4\pi g\mathbf{v}\delta(\mathbf{r}-\mathbf{v}t)\,. \tag{67}$$

The color index is omitted because it has a fixed direction in the color group space. The classical lowest-order solution of in-medium gluodynamics can be written as [111, 138]

$$\Phi^{(1)}(\mathbf{r},t) = \frac{2g}{\epsilon}\,\frac{\Theta(vt-z-r_\perp\sqrt{\epsilon v^2-1})}{\sqrt{(vt-z)^2-r_\perp^2(\epsilon v^2-1)}}\,, \tag{68}$$

and

$$\mathbf{A}^{(1)}(\mathbf{r},t) = \epsilon\mathbf{v}\Phi^{(1)}(\mathbf{r},t)\,, \tag{69}$$

where superscript (1) indicates solutions of the order $O(g)$ (the g-dependence of ϵ is not taken into account), $r_\perp = \sqrt{x^2+y^2}$ is the cylindrical coordinate, and z is the symmetry axis. These formulas describe both the space–time profile of the energy–momentum deposition and the dynamic response of the medium (the value of ϵ).

This solution describes the cone-like emission of Cherenkov gluons at the typical angle

$$\cos\theta = \frac{1}{v\sqrt{\epsilon}}\,. \tag{70}$$

It is constant for constant $\epsilon > 1$.

The expression for the radiation intensity is given by the Tamm–Frank formula [138] (up to the Casimir factors C_R)

$$\frac{\mathrm{d}E}{\mathrm{d}l} = 4\pi\alpha_{\rm s}C_R\int\omega\,\mathrm{d}\omega\left(1-\frac{1}{v^2\epsilon(\omega)}\right)\Theta\big(v^2\epsilon(\omega)-1\big)\,. \tag{71}$$

For absorbing media, ϵ acquires an imaginary part, the sharp front edge of shock wave (68) is smoothed, and the angular distribution of Cherenkov radiation widens. The δ-function of the angle (70) is replaced by the an angular shape à la Breit–Wigner [140–142] with the maximum at the same angle (for a small imaginary part of ϵ) and the width proportional to the imaginary part [see Eqn (78) below]. The special role of the $1/\epsilon$ factor in (68), which describes the wake left behind the parton, is discussed in Section 4.3.2.

We emphasize that this classical effect has a collective nonperturbative origin even though $\alpha_{\rm s}$ enters seemingly linearly in Eqn (71). The chromopermittivity ϵ accounts for nonperturbative terms responsible for the collective medium response. Only the emission of a primary gluon that triggers

this response is treated perturbatively; hence, the factor α_s appears in Eqn (71), but its effect is strongly enhanced and modified by the medium, as can be seen from the term in parentheses in the integrand.

4.3.1 Cherenkov gluons

A. The double-humped structure at the RHIC. The scalar and vector potentials in the momentum space can be written as

$$\Phi_a^{(1)} = 2\pi g Q_a \frac{\delta(\omega - kv\zeta)\, v^2\zeta^2}{\omega^2\epsilon(\epsilon v^2\zeta^2 - 1)}\,, \tag{72}$$

$$A_{z,a}^{(1)} = \epsilon v \Phi_a^{(1)}\,, \tag{73}$$

$$\zeta = \cos\theta\,, \tag{74}$$

where ω and k are the energy and momentum, and θ is the polar angle. We note again that both the Cherenkov term $(\epsilon v^2\zeta^2 - 1)^{-1}$ and the wake factor ϵ^{-1} are present.

The energy loss $\mathrm{d}W$ per length $\mathrm{d}z$ is determined by the formula

$$\frac{\mathrm{d}W}{\mathrm{d}z} = -gE_z\,. \tag{75}$$

In the lowest order,

$$E_z^{(1)} = \mathrm{i}\int \frac{\mathrm{d}^4k}{(2\pi)^4}\left[\omega A_z^{(1)}(\mathbf{k},\omega) - k_z\Phi^{(1)}(\mathbf{k},\omega)\right] \times \exp\left[\mathrm{i}(\mathbf{kv} - \omega)t\right]. \tag{76}$$

Inserting (72) and (73) into (76) and (75) gives (see also [143])

$$\frac{\mathrm{d}W^{(1)}}{\mathrm{d}z\,\mathrm{d}\zeta\,\mathrm{d}\omega} = \frac{g^2\omega}{2\pi^2 v^2\zeta}\,\mathrm{Im}\left[\frac{v^2(1-\zeta^2)}{1-\epsilon_\mathrm{t}v^2\zeta^2} - \frac{1}{\epsilon_\mathrm{l}}\right]. \tag{77}$$

The first term in the brackets corresponds to the transverse gluon Cherenkov radiation (the subscript t at ϵ_t) and the second term to the radiation due to the longitudinal wake (the index l at ϵ_l). The transverse and longitudinal components of the chromopermittivity tensor are explicitly indicated here, even though they are equal in any homogeneous medium.

Similarly to electrodynamics [140], the energy–angle spectrum of emitted gluons [141, 142] per unit length readily follows from (77) as

$$\frac{\mathrm{d}N^{(1)}}{\mathrm{d}\Omega\,\mathrm{d}\omega} = \frac{\alpha_s C\sqrt{x}}{2\pi^2}\left[\frac{(1-x)\,\Gamma_\mathrm{t}}{(x-x_0)^2 + (\Gamma_\mathrm{t})^2/4} + \frac{\Gamma_\mathrm{l}}{x}\right], \tag{78}$$

where

$$x = \zeta^2\,,\quad x_0 = \frac{\epsilon_{1\mathrm{t}}}{|\epsilon_\mathrm{t}|^2 v^2}\,,\quad \Gamma_j = \frac{2\epsilon_{2j}}{|\epsilon_j|^2 v^2}\,,\quad \epsilon_j = \epsilon_{1j} + \mathrm{i}\epsilon_{2j}\,. \tag{79}$$

The real (ϵ_1) and imaginary (ϵ_2) parts of ϵ are taken into account. The angle θ is the polar angle if the away-side jet axis is chosen as the z axis. It is clearly seen from Eqn (79) that the transverse and longitudinal parts of the chromopermittivity are responsible for distinctly different effects. The ringlike Cherenkov structure (conical emission) around this axis is clearly exhibited in the first term in (78). The second term defined by the longitudinal part of ϵ is responsible for the wake radiation described in Section 4.3.2.

We consider the first term. The angle θ is related to the laboratory polar (θ_L) and azimuthal (ϕ_L) angles in RHIC experiments as

$$x = \cos^2\theta = \sin^2\theta_L\cos^2\phi_L\,. \tag{80}$$

Integrating (78) over θ_L gives the final formula [141], to be compared with the two-hump structure of azimuthal (ϕ_L) correlations observed at the RHIC. The formula is quite lengthy and therefore not reproduced here. It can be seen already from (78) and (80) that this projection of the two-dimensional annulus on its diameter is symmetric about $\phi_L = \pi$ and exhibits humps whose positions are largely determined by ϵ_1 and whose widths are determined by ϵ_2. The first term in (78) clearly displays the Breit–Wigner angular hump, which replaces the δ-functional angular dependence characteristic for real ϵ (easily obtained from (78) as $\Gamma_\mathrm{t} \to 0$).

Actually, it is a matter of experiment to demonstrate whether Cherenkov gluons can be observed in some energy regions. No definite knowledge about the chromopermittivity or its exceeding 1, except the above conclusions, is available. Moreover, the absorption may be strong enough and hadronization (confinement) may change the final characteristics. The very first experimental indication in 1979 [137] that favored this effect dealt with a single cosmic ray event (some others, less pronounced, were also observed in cosmic rays and at lower energies in emulsion experiments at accelerators [144–157, 189]).

That is why it was a surprise when the so-called double-humped events in central nucleus–nucleus collisions were found at the RHIC in 2004 and confirmed later [158–168]. In fact, the obtained distributions closely resemble those published by Cherenkov in 1937 when he used the projection of famous rings on their diameter and got the double-humped structure (e.g., see [169]). We stress that this effect reflects an *intrinsic* property of the medium phenomenologically described by its permittivity ϵ.

Experimentalists at the RHIC used a quite elaborate method to learn about a parton passing through the quark–gluon medium. For two partons belonging to the colliding nuclei, we imagine large-angle scattering that occurs near the surface of the medium. The triggers placed at an angle about $\pi/2$ to the collision axis would register a normal jet created by a parton passing through the thin layer. Another scattered parton moves through the quark–gluon medium. Both partons produce jets. Two-particle correlations were studied. Those particles that belonged to the same jet formed a peak at low $\Delta\phi$. It was expected to detect a peak in the opposite direction at $\Delta\phi \approx \pi$ due to the correlation between particles from the trigger (near-side) and away-side jets. This was actually found in pp collisions, but not in central nucleus–nucleus collisions, which implied that the away-side jet is strongly modified when passing through the quark–gluon medium. For pions produced in some energy intervals, this could not be simply attributed to jet quenching because the two-hump structure appeared. Just this phenomenon was related to Cherenkov gluons.

In [141], a fit of this experimental data according to the formulas described above was performed and the values of the real and imaginary parts of the chromopermittivity were obtained. A Monte Carlo program was developed that took the specifics of collisions of initial partons and hadronization at the final stage (described by the transverse momentum

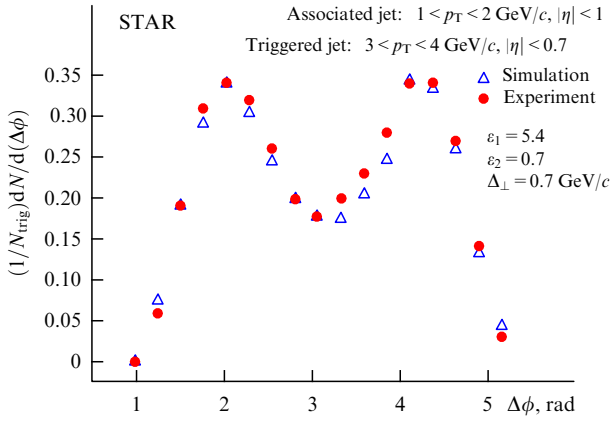

Figure 3. Associated azimuthal correlations at STAR: experiment: dots, theory: triangles.

spread parameter $\Delta_\perp$) into account. The fit to experimental data (with the elliptic flow subtracted) is shown in Fig. 3.

Thus, it was possible to determine the values of all three adjustable parameters (see Table 1). Constant values of $\epsilon_{1,2}$ were used because the interval of transferred momenta (frequencies) studied in experiment is quite narrow. Moreover, this assumption is directly supported by experiment (see [162–164, 170] for recent results), according to which the positions of peaks are independent of the transverse momenta of both the trigger (up to $p_T^{trig} = 6$ GeV) and associated particles (up to $p_T^{assoc} = 4$ GeV). This implies a constant ϵ_1 according to (78) and (79).

The initial results differed for STAR and PHENIX because of a disagreement over the respective positions of the peaks (mostly determined by ϵ_1), $\pi \pm 1.04$ and $\pi \pm 1.27$, and the widths (mostly determined by ϵ_2). The new data [170, 171] give $\pi \pm 1.1$, and hence $\epsilon_1 \approx 6$ and $\epsilon_2 \approx 0.8$ would be good estimates, as can be guessed from the range of values in Table 1. The principal conclusion about the large values of ϵ_1 indicating nongaseous matter with large N_s in Eqn (64) is supported in any case. The imaginary part of the chromopermittivity is comparatively small relative to the real part. Low attenuation helps observe this effect.

The experimental data show that the often cited[10] conclusion in [124] about smaller angles for larger p_T is wrong. The model of a single scalar resonance used there for the derivation of the dispersion equation defining the energy dependence of the chromopermittivity is oversimplified. This defect can be cured by the set of overlapping resonances from PDG, which leads to an approximately constant ϵ in the low-energy region cut off by the Hagedorn temperature if formula (64) is used. This set of resonances can be used to model the collective excitations of the quark–gluon medium analogously to excited levels of atoms in electrodynamics [114]. The energy loss per Fm can be estimated according to Eqn (71) as about C_R [GeV] if the resonance region ends at 4 GeV. The loss depends on this parameter quadratically, bringing some flexibility to the estimate, which nevertheless shows that they are rather large.

Table 1.

Experiment	θ_{max}	ϵ_1	ϵ_2	$\Delta_\perp$, GeV	New data
STAR*	1.04 rad	5.4	0.7	0.7	$\theta_{max} \approx 1.1$ rad
PHENIX**	1.27 rad	9.0	2.0	1.1	$\epsilon_1 \approx 6$, $\epsilon_2 \approx 0.8$

* Solenoidal Tracker At RHIC.
** Pioneering High-Energy Nuclear Interaction eXperiment.

For three-particle correlations [171–173], the peak was at large angles according to the initial data. But the latest data in [171] agree with the above-described estimates. These correlations also show that the hypothesis about deflected jets [174] is not valid because off-diagonal peaks are seen in the experiment, which cannot appear according to this hypothesis. The presence of such peaks is evidence of a conical emission pattern.

In-medium modifications of QCD bremsstrahlung calculations (see, e.g., [175]) predicted some broadening of the away-side peak, but this was insufficient for obtaining the double-humped structure after subtracting the collective flow v_2 effects.

In principle, the two-hump structure may arise not only due to Cherenkov gluons but also as a sonic Mach cone [176–178]. In contrast to gluodynamics, it is ascribed to *longitudinal* excitations in plasma [178, 125]. The model with a hypothesized space-like dispersion relation

$$\omega = \sqrt{u^2 k^2 + \omega_p^2} \tag{81}$$

was considered in [125]. Here, ω_p denotes the plasma frequency, and u is the speed of a plasmon. The model describes a Mach shock wave for a supersonic source. Similar structures appeared in models reliant on the AdS/CFT correspondence [179, 180].

In 3D hydrodynamics with large local density fluctuations that have the form of tubes at the initial moment,[11] both the ridge and the double-humped structures arise [181–183]. They appear only if the combination of these special nonsmooth initial conditions with the hydrodynamic evolution of the hot and dense medium is used such that the tubes induce the appearance of ridges in the hydrodynamic flow. At the same time, as was shown in [184], in hydrodynamics with somewhat different and less special initial conditions, the particle yield from the *transverse* wake moving opposite to the trigger jet largely overwhelms the weak Mach cone signal for relativistic particles.[12] The jet of particles in this direction should appear (the strong away-side jet), but is not observed in experiment. As shown in Section 4.3.2, this effect does not take place in chromodynamics, where the *longitudinal* wake [the second term in Eqn (78)] results in emission perpendicular to the parton trail. The hydrodynamic Mach cone interpretation has not yet been used for quantitative fits of experimental data aimed at obtaining information on the medium properties.

The charge orientation in color space is fixed in the classical equations of gluodynamics. There is no color dependence in their solutions, other than trivial Casimir factors, which just determine the overall normalization. Therefore, the statement that "their absence... in 'conical

[10] E.g., "the Cherenkov angle *decreases* with the momentum of the radiated gluon" [38].

[11] Does it not bring to mind the field tubes in Glasma described above?

[12] This conclusion differs from those in [181–183], where no away-side signal at $\Delta\phi = \pi$ is seen. Probably, this is due to the choice of a single high-density spot in the initial conditions of the hydrodynamic model, while two partons are necessarily created in the parton treatment.

flow' suggests *sound radiation* rather than the gluonic one" [185] is entirely unjustified. The functional color dependence may appear in gluodynamics as an effect at higher orders (see Section 4.5).

Several attempts have been made to ascribe the double-humped structure around away-side jets to the large-angle emission of shower gluons [174, 185] or to their deflection due to random multiple scattering [186] or coupling to collective flows [187, 188], but they require additional ad hoc parameters with values that are not compatible with experiment [162–164]. The collective medium behavior as the origin of the humps is clearly seen from the properties of hadrons inside the shoulder regions (p_T- and centrality-independent shapes, mean p_T, composition) being similar to those observed for inclusive processes [162–164]. Their energy dependence suggests stronger medium effects at higher energies, as expected in [162–164].

The method of wavelet analysis was successfully applied to distinguish between jets and conical structures in three-dimensional plots on an event-by-event basis [189, 190].

It was assumed everywhere above that the direction of gluons defines the direction of final pions. The new mechanism of direct emission of Cherenkov *mesons* by *heavy* quarks was considered in the effective theory involving the gauge/gravity duality [127]. The Cherenkov angle is the same, but is determined by the mass ratio, i.e., by the kinematics alone, without any reference to medium properties (chromopermittivity).

B. The asymmetry of in-medium resonances (SPS, etc.). The necessary condition for Cherenkov effects to be observable within some energy interval is $\epsilon(\omega) > 1$ for ω belonging to this interval. According to Eqn (64), this implies that $\mathrm{Re}\, F_0(\omega) > 0$. This requirement is satisfied within the low-energy (left) wings of resonances described by the Breit–Wigner formula. Therefore, the collective excitations of the quark–gluon medium leading to Cherenkov gluons can be expected to produce a certain effect in addition to the traditional resonance effects in these energy intervals. Hence, the general prediction follows that the shape of *any* resonance formed in nucleus collisions must become asymmetric, with some excess within its left wing compared to the usual Breit–Wigner shape. Because the probability of Cherenkov radiation is proportional to $\Delta\epsilon = \epsilon - 1$, this asymmetry must be proportional to $\rho(\omega)$. Experimentally, one of the best ways to observe it is, e.g., to measure the dilepton mass distribution of the corresponding modes of resonance decays. Then this distribution must have the shape [191]

$$\frac{\mathrm{d}N_\mathrm{l}}{\mathrm{d}M} = \frac{A}{(m_\mathrm{r}^2 - M^2)^2 + M^2\Gamma^2} \times \left[1 + w_\mathrm{r}\,\frac{m_\mathrm{r}^2 - M^2}{M^2}\,\Theta(m_\mathrm{r} - M)\right], \qquad (82)$$

where M is the dilepton mass and m_r is the resonance mass. The first term corresponds to the ordinary Breit–Wigner cross section with a constant normalization factor A. According to the optical theorem, it is proportional to the imaginary part of the forward scattering amplitude. The second term describes the coherent Cherenkov response of the medium proportional to the real part of the amplitude. Its contribution relative to ordinary processes is described by the only adjustable parameter, w_r, for a given resonance r, which must be found from comparison with experimental data .

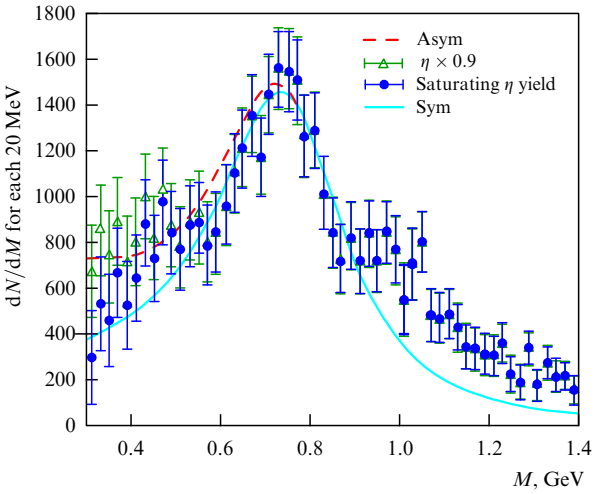

Figure 4. Modified spectrum of dileptons in semicentral collisions In(158 A GeV)–In for NA60 (points) compared to the ρ-meson peak in the medium with an additional Cherenkov contribution (dashed line).

This formula has been compared with the most accurate experimental results [192] on the dilepton spectra of the ρ-resonance produced in nucleus collisions at the SPS (see Fig. 4). An asymmetry of the dilepton mass spectrum is clearly seen. The corresponding parameter w_ρ was found to be equal to 0.19. This confirms the above conclusion that the contribution of Cherenkov effects is not negligible and stresses the fact that resonance regions may be responsible for it at rather low energies. This feature is well known in electrodynamics (see, e.g., Fig. 31-5 in [114]), where atoms behaving as oscillators radiate as Breit–Wigner resonances when excited.

Presently, numerous data exist on other resonances produced in nucleus collisions with qualitative indications of the asymmetry of their shapes with an excess of low-mass wings [193–197]. This agrees with the universal prediction of Eqn (82).

C. Cosmic ray events. The very first events exhibiting a ring-like structure were observed in nontrigger cosmic ray experiments. Just they initiated the idea about Cherenkov gluons [133]. Two peaks more densely populated by particles than their surroundings were noticed in the cosmic ray event [137] initiated by a primary with an energy about 10^{16} eV, close to LHC energies.

The distribution in the number of particles produced is shown in Fig. 5, where it is plotted as a function of the distance from the collision axis proportional to the polar angle θ. It clearly shows two maxima. This event was registered in a detector with nuclear and X-ray emulsions during a balloon flight at an altitude about 30 km. At the early stages, the idea about clusters (fireballs, clans, jets, etc.) was proposed, but it failed to explain the data. At approximately the same time, a similar event with two peaks was observed at 10^{13} eV [144]. Some events with one peak (due to the limited acceptance of the installation?) were shown even earlier [145–147]. When the two-dimensional distribution of particles was considered in the azimuthal plane (called the target diagram in cosmic ray experiments), this event revealed two (forward and backward in c.m.s.) densely populated ring-like regions within two narrow intervals of polar angles (corresponding to

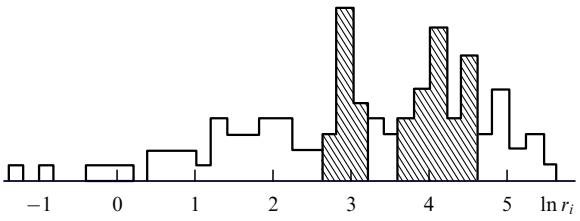

Figure 5. The distribution of the number of produced particles at different distances from the collision axis r in a stratospheric event at 10^{16} eV [136] has two pronounced peaks. Correspondingly, the distribution in pseudorapidity also has two such peaks.

peaks in Fig. 5) but widely distributed in azimuthal angles for each of them. Such events were therefore termed ring-like events. The peaks were interpreted as effects due to Cherenkov gluons emitted by the forward and backward moving initial high-energy partons. In cosmic ray events, the energies of partons are high and the effect can be related to the high-energy behavior of $\mathrm{Re}\, F_0(E)$.

It is important to note that the energies of particles produced within the humps (rings) in RHIC data are rather low on the scale of initial energies. Even the energies of parent jets in the double-humped events are lower than 5 GeV. Therefore, the whole effect at the RHIC can be related to the low-energy region.

One of the most intriguing problems is how to properly understand the fact that the RHIC and cosmic ray data were fitted with very different chromopermittivity values, respectively close to 6 and 1. This could be interpreted as being due to the difference in the values of x (the parton share of energy) and Q^2 (the transverse momenta squared) and the Lorentz transformations into different rest frames. It is well known that the region of large x and Q^2 corresponds to a dilute partonic system. At low x and Q^2, the density of partons is much higher. Hence, the effective values of N_s in (64) are different.

As follows from the estimate based on Eqn (64) [198, 199], the density of scattering centers under RHIC conditions is very high: about ten partons per proton volume. In this case, we are dealing with rather low x and Q^2. Therefore, we should expect a high density of partons in this region and a large $\Delta\epsilon$. It is interesting to note that the two-hump structure disappears in the RHIC data at higher p_T, where the parton density becomes much lower. This corresponds to smaller ϵ and θ, i.e., humps merge in the main away-side peak.

In the cosmic ray event, the observed effect is associated with the leading large-x partons. In addition, experimentalists pointed out that the transverse momenta in this event are quite large. In this region, a low parton density and very small $\Delta\epsilon$ can be expected. In contrast to a single parton traversing the medium at the RHIC energies, the collision of forward moving partons at the LHC can be regarded as the collision of two relatively dilute *bunches* of partons. Nevertheless, the macroscopic approach is valid there as well.

Thus, the same medium can probably be considered as a liquid or a gas depending on the parton energy and transferred momenta. This statement can be verified experimentally by using triggers positioned at different angles to the collision axis[13] and considering different transverse momenta. In this way, the hadronic Cherenkov effect can be used as a tool to scan the $(1/x, Q^2)$ plane and plot the parton densities corresponding to its different regions.

4.3.2 The wake. In central collisions, the interaction region is symmetric and the change of the trigger position might lead to some effect only if the chromopermittivity strongly depends on ω. This is not likely to be the case for narrow energy intervals. But in mid-central nuclear collisions, the interaction region itself becomes asymmetric, reminiscent of a rugby ball. Therefore, new effects can appear when the angular position of the trigger is changed. It has been found (see Figs 2 and 3 in [171]) that a similar two-hump structure appears, but with some additional contribution noticeable at a particular orientation of the trigger particle just between the in-plane and out-of-plane directions.[14] It was stated in [171] that "at present, it is unclear whether this merely reflects a geometry dependent shift in the away-side peaks or perhaps an additional contribution at $\Delta\phi = \pi/2$."

We have argued [142] that this is an additional contribution in the vicinity of $\Delta\phi = \pi/2$, known in electrodynamics as the wake effect (see, e.g., [200]). At the same time, it is strongly influenced by the special geometry of mid-central collisions in such a way that the wake radiation at about the $\pi/4$-orientation of the trigger particle can escape the overlap region much more easily than wake gluons for in-plane and out-of-plane orientations of the trigger particle.

According to Eqn (78), the second term corresponds to the radiation induced by the longitudinal oscillations in the wake left behind the away-side parton. It is emitted mostly in the direction perpendicular to the wake. That resembles the dipole radiation. Just the color charge-changing regions of a dipole-like structure behind the parton are seen in Monte Carlo simulations of the wake [201, 202] trailing the color parton. The enhanced and depleted charge density regions alternate. The $1/\sqrt{x}$ singularity is stronger than the $\sin^2\theta$ dipole distributions, however, and must somehow be saturated in the vicinity of $x = 0$ by the spatial dispersion of ϵ. Therefore, this term can be used for qualitative conclusions only in the region not very close to $x = 0$.

The estimates [142] of the relative importance of the two terms in Eqn (78) show that the wake radiation is negligible at the peak of the Cherenkov humps at $x = 0$. But the two terms become comparable at

$$x_e \approx \frac{x_0^2}{2x_0 + 1}\,, \tag{83}$$

which corresponds to the angles $\pi - \Delta\phi_L \approx 1.43$ rad. The wake radiation overwhelms the Cherenkov contribution at $\Delta\phi_L < \pi - 1.43$ rad, where the latter decreases. Therefore, the shift of their combined maximum to $\pi - \Delta\phi_L \approx 1.3$ rad noticed in [171] and shown in Fig. 2 in that paper seems quite plausible if explained as the effect of the wake.

We note the difference between Cherenkov and wake radiations. The name 'wake' is sometimes attributed to both of them [125, 178]. However, it can be shown [142, 200] that the trail behind the parton (the wake) induced by the chromopermittivity corresponds just to the second term in (78). Moreover, the wake radiation exists only for a nonzero imaginary part of ϵ_1, while the Cherenkov radiation also exists and acquires the traditional δ-functional angular shape for real ϵ. The effect of a transverse wake in

[13] An example is described in Section 4.3.2.

[14] This plane is defined by the collision axis and the impact parameter.

hydrodynamics is completely different. It produces a strong peak in the away-side direction at $\Delta\phi_{\rm L} = \pi$ [184], which is not observed in experiment.

4.3.3 Transition radiation. In 1945, Ginzburg and Frank proposed the idea of transition radiation [203]. Any electric charge passing from some medium to another or moving with an (almost) constant velocity in an inhomogeneous medium with a variable dielectric permittivity induces its polarization and radiation of photons. This property has been used, for example, to build the transition radiation tracker in the ATLAS (A Toroidal LHC ApparatuS) detector at the LHC. The transition radiation is determined by restructuring the electromagnetic field surrounding the electric charge.

During hadron (nucleus) collisions, the partons intersect the surface of the partner particle (nucleus). This transition should induce abrupt changes in their color fields and, consequently, radiation of gluons. The classical in-medium QCD equations coincide in their general structure with the electrodynamic equations. Because this approach turned out to be successful with Cherenkov gluons and wakes, it is tempting to apply the Ginzburg–Frank formula to estimate the number of gluons emitted per unit length within some frequency and angular intervals:

$$\frac{{\rm d}N}{{\rm d}\omega\,{\rm d}\Omega} = \frac{\alpha_{\rm s}\sqrt{\epsilon_a}\sin^2 2\theta}{\pi\omega} \times \left| \frac{(\epsilon_b-\epsilon_a)(1-\epsilon_a+\sqrt{\epsilon_b-\epsilon_a\sin^2\theta})}{(1-\epsilon_a\cos^2\theta)(1+\sqrt{\epsilon_b-\epsilon_a\sin^2\theta})(\epsilon_b\cos\theta+\sqrt{\epsilon_a\epsilon_b-\epsilon_a^2\sin^2\theta})} \right|^2 , \tag{84}$$

where $\epsilon_{a,b}$ are the chromopermittivities of the media a, b as felt by relativistic ($v \approx c$) partons traversing the surface when passing from b to a. In (84), we have omitted the color Casimir factors.

There is an important difference between Cherenkov and transition radiations. Cherenkov radiation can be observed only if the particle moves in a medium with $\epsilon > 1$. The radiation intensity is proportional to $\epsilon - 1$ according to (71). Transition radiation is proportional to $(\epsilon_b - \epsilon_a)^2$ [see (84)] and appears at any change in ϵ. In electrodynamics, it is studied mostly in the frequency interval where formula (63) is applicable, i.e., where $\Delta\epsilon < 0$. Just this behavior of the dielectric permittivity is responsible for specific features of transition radiation. In the case of the nuclear medium, it is unknown whether an analogous formula can be used in any energy region. For narrow energy intervals, it is reasonable to assume $\Delta\epsilon$ to be constant. At very high energies, dependence (66) may be used. Both these assumptions find some support in the RHIC and cosmic ray data, as discussed above. That is why we consider these two possibilities first [204].

An away-side parton is created at the RHIC inside the quark–gluon medium, moves through it, and escapes into the vacuum, where it hadronizes. According to the above estimates, $\epsilon_b \approx 6 \gg \epsilon_a = 1$. Using (84), we obtain a bremsstrahlung-like spectrum with both infrared and collinear divergencies in asymptotic regimes,

$${\rm d}N \propto \frac{{\rm d}\omega}{\omega}\,\frac{{\rm d}\theta}{\theta}\,. \tag{85}$$

At finite energies, the angular divergence is replaced by the maximum at $\theta \approx \gamma^{-1}$. Anyway, this radiation is collimated near the initial direction of the away-side parton and is hard to detect because of the strong background. Similar conclusions are obtained in [205] for the radiation by a gluon moving in a stochastic medium. It is interesting to note that for $\epsilon_b \gg \epsilon_a$, the transition radiation intensity in (85) is independent of ϵ_b.

According to (66), for forward moving partons with extremely high energies, the deviation of chromopermittivity from unity is very small. Then

$${\rm d}N \propto \frac{{\rm d}\omega}{\omega^5}\,\frac{{\rm d}\theta}{\theta}\,\Theta(\omega-\omega_{\rm th})\,. \tag{86}$$

The collinear divergence remains the same, but the energy spectrum acquires a strong peak near $\omega_{\rm th}$. This implies that resonance-like, nearly monochromatic subjets with masses close to $\omega_{\rm th}$ must be produced at the LHC energies. These 'resonances' are mostly created by gluons and are therefore neutral. The most favored channel would be to observe them as peaks in mass spectra of forward moving $\mu^+\mu^-$ pairs near $\omega_{\rm th}$. Unfortunately, no clear prescription exists for translating the threshold energy in hadronic reactions to gluons. If observed, peak locations and their disappearance at $\omega = \omega_{\rm th}$ due to $\Theta(\omega - \omega_{\rm th})$ would yield information about that.

It may be hoped that the confinement and hadronization do not spoil these conclusions. This is supported by the observation of effects due to Cherenkov gluons. But the transition radiation might be more strongly influenced by confinement near the QGP surface than collective excitations in the bulk. On the one hand, this shortens the radiation length, but on the other hand, the abrupt variation of color fields surrounding partons when they come out of the quark–gluon plasma and hadronize may enhance the transition radiation because of strong confining forces. At the same time, the transition radiation may appear in much wider energy intervals than Cherenkov radiation (in particular, at $\omega < \omega_{\rm th}$). However, neither experimental nor theoretical arguments about the chromopermittivity in these regions are presently available. It would not be surprising if we find its effects outside the regions where the double-humped events were observed. That may somewhat smoothen down the structures near $\omega_{\rm th}$.

Another way to account for the difference between vacuum and medium chromopermittivities is to consider different masses of gluons and values of the running coupling in these two environments. This was done in [126, 128, 129], where the transition radiation of heavy quarks was treated within a microscopic approach. It was shown that transition radiation can be as important as the induced gluon radiation. However, the conclusions are still indefinite because of strong cancellation effects and assumptions about the behavior of the coupling constant.

We also note the important problem of the finite size L of hadronic objects. It necessarily induces (see, e.g., [126, 130, 134, 206]) factors like $1 - \cos L/L_0$ in emission probabilities. Estimates of the scale length L_0 are still not very definite. This problem is closely connected with decisions about the radiation (formation) lengths and/or about the points where the partons were created.

4.4 Instabilities at high energies

The tachyonic-type model (66) proposed for the chromopermittivity at high energies is inevitably related to instabilities in

the quark–gluon medium. The dielectric permittivity of the macroscopic matter [e.g., as given by (63)] is usually considered in its rest frame, which is well defined. For collisions of two nuclei (or hadrons), such a system requires a special definition (see [111, 207]). In particular, for fast forward moving partons, the partons of another (target) nucleus, which is at rest, are spectators (medium). We therefore consider the problem of a system of the quark–gluon medium impinged by a bunch of fast partons similarly to the problem of plasma physics, namely, that of the interaction of an electron bunch with a plasma [208–210]. This differs from RHIC conditions, where partons scattered at $\pi/2$ were regarded as moving in the medium with its rest frame coinciding with the center-of-mass system of the nuclei.

Two complications are to be considered. First, there are preferred directions of the current (z axis) and its radiation. This is solved by introducing the permittivity tensor as

$$D_i(\omega,\mathbf{k}) = \epsilon_{ij}(\omega,\mathbf{k})\, E_j(\omega,\mathbf{k})\,. \tag{87}$$

Second, the impinging bunch content is similar to that of the target (plasma–plasma collisions!), and its permittivity must also be accounted for. In the projectile system, it is the same as the permittivity of the target in its rest frame i.e., given by (66). Next, using the fact that the total induced current is the sum of currents induced in the target, we must Lorentz-transform the projectile internal fields, polarization vector, and currents to the target rest frame, where we consider the whole process. In this way, the Lorentz transformation of the conductivity tensor $\sigma_{ij}(\omega,\mathbf{k})$ [and, correspondingly, of $\epsilon_{ij}(\omega,\mathbf{k})$] is found as was done in [208–212]. Using the current conservation and classical field equations (58) and (59) with $g=0$, we obtain the nonzero components of the chromopermittivity tensor as

$$\begin{aligned}
\epsilon_{xx} &= \epsilon_{yy} = 1+\frac{\omega_0^2}{\omega^2}\left(1+\frac{1}{\gamma}\right),\\
\epsilon_{xz} &= -\epsilon_{zx} = \frac{\omega_0^2 k_\mathrm{T}}{\omega^2(\omega-k_z)\,\gamma}\,,\\
\epsilon_{zz} &= 1+\frac{\omega_0^2}{\omega^2}\left(1+\frac{k_\mathrm{T}^2}{(\omega-k_z)^2\gamma}\right),
\end{aligned} \tag{88}$$

where k_T and k_z are the transverse and longitudinal components of $\mathbf{k}$. We use the approximation of high energies (a large $\gamma \gg 1$ factor, i.e., $v\approx 1$). The terms depending on γ are due to the impinging partons. They can be omitted everywhere except in terms that determine the Cherenkov gluon radiation at $\omega - k_z \approx 0$.

The classical equations derived from (60) and (61) and written in the momentum space have a solution if the dispersion equation

$$\det(\omega,\mathbf{k}) = |k^2\delta_{ij} - k_i k_j - \omega^2\epsilon_{ij}| = 0 \tag{89}$$

holds,which is of the sixth order in the momentum. However, the sixth-order terms cancel and (89) leads to two (second-order) equations

$$k^2-\omega^2-\omega_0^2 = 0\,, \tag{90}$$

$$(k^2-\omega^2-\omega_0^2)\left(1+\frac{\omega_0^2}{\omega^2}\right) - \frac{\omega_0^4 k_\mathrm{T}^2}{\omega^2(\omega-k_z)^2\gamma} = 0\,. \tag{91}$$

They respectively determine the internal modes of the medium and the bunch propagation through the medium.

Equation (90) shows that the quark–gluon medium is unstable because a branch with $\mathrm{Im}\,\omega > 0$ exists for modes $k^2 < \omega_0^2$. Therefore, the energy increase in the total cross sections responsible for the positiveness of $\mathrm{Re}\,F_0(\omega)$ at high energies is related to the instability of the quark–gluon medium.

Equation (91) has solutions corresponding to Cherenkov gluons emitted by the impinging bunch and determined by the last term in (91). They can be found at $\omega = k_z + \delta$ ($\delta \ll \omega$). For $k_\mathrm{T} = \omega_0$, we obtain solutions with

$$\mathrm{Im}\,\delta_1 = \frac{\omega_0^2}{2k_z\left[2\gamma(1+\omega_0^2/k_z^2)\right]^{1/3}}\,. \tag{92}$$

For $k_\mathrm{T} \neq \omega_0$, there is a solution with

$$\mathrm{Im}\,\delta_2 = \frac{\omega_0^2 k_\mathrm{T}}{k_z\left[\gamma|k_\mathrm{T}^2-\omega_0^2|(1+\omega_0^2/k_z^2)\right]^{1/2}}\,. \tag{93}$$

It is well known (see [138]) that the solutions of dispersion equation (89) determine the Green's function for the equations of the system,

$$G(t,z) = \frac{1}{2\pi^2}\int_{-\infty}^{\infty}\mathrm{d}k\int_{C(\omega)}\frac{1}{\det(\omega,\mathbf{k})}\exp\left(-\mathrm{i}\omega t+\mathrm{i}kz\right)\mathrm{d}\omega\,, \tag{94}$$

where the contour $C(\omega)$ passes above all singularities in the integral. Therefore, a positive $\mathrm{Im}\,\delta_i$ in (92) and (93) corresponds to the absolute instability of the system. We note that the instability at $k_\mathrm{T}=\omega_0$ is stronger than at $k_\mathrm{T}\neq\omega_0$ by approximately the factor $\gamma^{1/6}$ (this factor is about 4 times larger at the LHC than at the RHIC). Instability exponent (92) decreases as $\gamma^{-1/3}$ and is about 16 times smaller at the LHC than at the RHIC. It asymptotically tends to zero.

Thus, Cherenkov gluons are emitted with a constant transverse momentum $k_\mathrm{T}=\omega_0$ and their number, at high energies, is proportional to

$$\frac{\mathrm{d}\omega}{(\omega)^2}\,\Theta(\omega-\omega_\mathrm{th})\,,$$

because $\epsilon(\omega)$ is given by Eqn (66) with reference to the threshold above which this equation is applicable. It differs from the traditional folklore of a constant emission angle of Cherenkov radiation and the number of gluons $\propto \mathrm{d}\omega$ (or the total energy loss proportional to $\omega\,\mathrm{d}\omega$). This difference is easily explained by Eqns (70) and (71), which give $\cos\theta = \mathrm{const}$ and the energy loss $\omega\,\mathrm{d}\omega$ for $\epsilon = \mathrm{const}$ and $k_\mathrm{T}\approx\omega_0$ and $\mathrm{d}\omega/\omega$ for $\epsilon = 1+\omega_0^2/\omega^2$.

If the data about $\mathrm{Re}\,F_0(\omega)$ for hadronic processes are used in (64) and fitted by (66), then the value of ω_0 depends on the density of scatterers N_s, and with the above estimates can be of the GeV order.

4.5 Nonlinear effects and the color rainbow

In Eqns (60) and (61) for in-medium QCD considered in Section 4.1, the chromopermittivity was assumed to be Abelian, $\epsilon^{ab} = \delta^{ab}\epsilon$. The simplest generalization of Eqns (60) and (61) taking the non-Abelian properties of the chromopermittivity ϵ^{ab} into account uses the tensor structure of ϵ^{ab}. We write the corresponding generalization of (60) and (61) in

the leading order in the coupling constant:

$$\triangle \mathbf{A}^a - \epsilon^{ab}\,\frac{\partial^2 \mathbf{A}^b}{\partial t^2} = -\mathbf{j}^a\,,$$
$$\epsilon^{ab}\left(\triangle \Phi^b - \epsilon^{bc}\,\frac{\partial^2}{\partial t^2}\,\Phi^c\right) = -\rho^a\,, \qquad (95)$$

where $(\rho^a, \mathbf{j}^a)$ are the components of the external color current j^a_μ defined in (67).

From the physical meaning of the chromopermittivity ϵ^{ab},[15] it follows that its most general expression is a symmetric tensor $\epsilon^{ab} = \epsilon^{ba}$ with equal diagonal $\epsilon^{(\mathrm{d})}$ and off-diagonal $\epsilon^{(\mathrm{o})}$ components. To elucidate the physical content of Eqns (95), we consider a similarity transformation U diagonalizing the matrix ϵ^{ab}:

$$\epsilon \to \tilde{\epsilon} = U\epsilon U^{-1}\,. \qquad (96)$$

In (96), the matrix $\tilde{\epsilon}$ is the diagonal matrix whose elements are the eigenvalues of the chromopermittivity tensor $\{\epsilon^{(a)}\}$, $a = 1, \ldots, N_c^2 - 1$. It is easy to show that under the above assumptions on the structure of ϵ^{ab}, we have

$$\epsilon^{(1)} \equiv \epsilon^* = \epsilon^{(\mathrm{d})} + 2\epsilon^{(\mathrm{o})}\,,$$
$$\epsilon^{(2),\ldots,(N_c^2-1)} \equiv \epsilon^{**} = \epsilon^{(\mathrm{d})} - \epsilon^{(\mathrm{o})}\,. \qquad (97)$$

The rotation U allows diagonalizing (95) in terms of the modified fields $\tilde{A}^a_\mu = U^{ab}A^b_\mu$ and the modified current $\tilde{j}^a_\mu = U^{ab}j^b_\mu$:

$$\triangle \tilde{\mathbf{A}}^a - \epsilon^{(a)}\,\frac{\partial^2}{\partial t^2}\,\tilde{\mathbf{A}}^a = -\tilde{\mathbf{j}}^a\,,$$
$$\triangle \tilde{\Phi}^a - \epsilon^{(a)}\,\frac{\partial^2}{\partial t^2}\,\tilde{\Phi}^a = -\frac{\tilde{\rho}^a}{\epsilon^{(a)}}\,. \qquad (98)$$

The structure of eigenvalues in (97) implies the existence of two different solutions of Eqns (98), corresponding to the eigenvalues $(\epsilon^*, \epsilon^{**})$,

$$\tilde{\Phi}^{(1)\,1}(\mathbf{r}, t) = \frac{2g}{\epsilon^*}\,\frac{\Theta(vt - z - r_\perp\sqrt{\epsilon^* v^2 - 1})}{\sqrt{(vt-z)^2 - r_\perp^2(\epsilon^* v^2 - 1)}}\,,$$
$$\tilde{\Phi}^{(1)\,2,\ldots,N_c^2-1}(\mathbf{r}, t) = \frac{2g}{\epsilon^{**}}\,\frac{\Theta(vt - z - r_\perp\sqrt{\epsilon^{**} v^2 - 1})}{\sqrt{(vt-z)^2 - r_\perp^2(\epsilon^{**} v^2 - 1)}}\,, \qquad (99)$$

and similar solutions for $\tilde{\mathbf{A}}^a$. Returning to the original fields $A^a_\mu = (U^{-1}\tilde{A})^a_\mu$ evidently gives the solution corresponding to the presence of a color Cherenkov rainbow formed by Cherenkov radiation at the angles

$$\cos\theta^* = \frac{1}{v\sqrt{\epsilon^{(\mathrm{d})} + 2\epsilon^{(\mathrm{o})}}}\,, \quad \cos\theta^{**} = \frac{1}{v\sqrt{\epsilon^{(\mathrm{d})} - \epsilon^{(\mathrm{o})}}}\,. \qquad (100)$$

In the limit $\epsilon^{(\mathrm{o})} \ll \epsilon^{(\mathrm{d})}$, solution (99) turns into the standard solution (67), (68).

To account for nonlinear contributions to the in-medium Yang–Mills equations, it is necessary to use the corresponding generalizations of (95). In [207], to demonstrate the possible practical consequences of such an approach, the procedure of model calculations of the nonlinear contributions to the gluon Cherenkov radiation was described, albeit with some simplified (and nonrealistic) assumptions regarding the color structure of the chromopermittivity. It was shown that in the case under consideration, the solutions acquire contributions of the form

$$\propto \frac{\Gamma_\mathrm{t}\sqrt{x}}{[(x - x_0)^2 + (\Gamma_\mathrm{t})^2/4]^{5/4}}$$

and

$$\propto \frac{\Gamma_\mathrm{t}}{\sqrt{x}[(x - x_0)^2 + (\Gamma_\mathrm{t})^2/4]^{3/4}}\,,$$

which correspond to the color rainbow and differ (despite some similarity) from the lowest-order solution (78).

4.6 Hydrodynamics (thermodynamic and mechanical properties of quark–gluon plasma)

The chromodynamic properties of QGP described above are its average characteristics measured by a test parton. Therefore, they are more robust than the thermodynamic and mechanical characteristics, which change during the evolution of the quark–gluon medium and whose assessment requires spatial and temporal information. The lattice calculations and ideas about CGC, Glasma, and QGP provide some hints regarding the transition from the confined state to deconfined quarks and gluons. Inelastic collisions may lead to thermalization of the medium. Subsequently, it expands and hydrodynamics may be applied to treat this stage of evolution. This is described in many reviews (see [109, 110]), and we give just a brief survey of it here.

The medium is characterized by six independent variables: the energy density e, the pressure p, the baryon number n_B, and three components of the velocity vector u_μ. The energy–momentum tensor and the baryon number current are

$$T^{\mu\nu}(x) = \big(e(x) + p(x)\big)\,u^\mu(x)\,u^\nu(x) - p(x)\,g^{\mu\nu}\,,$$
$$j^\mu_\mathrm{B}(x) = n_\mathrm{B}(x)\,u^\mu(x)\,. \qquad (101)$$

The evolution of these variables is described by six equations of hydrodynamics: five nonlinear partial differential equations obtained from local conservation laws for energy, momentum, and baryon number,

$$\partial_\mu T^{\mu\nu}(x) = 0\ (\nu = 0, \ldots, 3), \quad \partial_\mu j^\mu_\mathrm{B}(x) = 0\,, \qquad (102)$$

and an equation of state relating p, e, and n_B. The equation of state is usually chosen in the closest possible form to the results of lattice QCD by normalization on the states below and above the critical temperature (i.e., of hadrons and the quark–gluon medium). This is a rather arbitrary element of the whole approach. In addition, solutions of the nonlinear equations in $3+1$ dimensions require initial conditions to be defined and may only be obtained numerically with several external parameters. This is the origin of several conflicting results, as was discussed above with reference to [125, 176–178, 181, 182, 184]. The CGC and Glasma approaches provide some guesses about the initial conditions for the evolution of a thermalized QGP. However, the evolution of the Glasma into a thermalized QGP is not yet understood.

At least four parameters are necessary to fix the initial conditions and the freeze-out algorithm that determines the transition from the hydrodynamic characteristics to the

[15] In this subsection, we consider the simplest case of real chromopermittivity.

hadronic stage: the initial time τ_{eq}, the energy (or entropy) density s_{eq}, the baryon number $n_{B,eq}$, and the freeze-out temperature (or decoupling energy density) e_{dec}. They are fixed by comparison of theoretical results with experimental data. Schematically, the correspondence of these parameters and experimental characteristics can be represented as $dN/dp_T - T - e_{dec}$, $dN/dy - (\tau s)_{eq}$, $p/\pi - n_{B,eq}/s_{eq}$, and $(dN/dp_T)_p/(dN/dp_T)_\pi - \tau_{eq}$. Moreover, the overlap geometry of the two colliding nuclei allows defining the shape of the initial density profiles, as well as making assumptions concerning the profiles of the initial longitudinal and transverse flows and the prescription for final hadronization.

Solutions of the hydrodynamic equations yield the transverse momentum spectra for various species of particles, the radial and elliptic flows, and the shape of the interaction region (as revealed by Bose–Einstein correlations and Hanburry Brown–Twiss interferometry). Their comparison with experimental data allows determining the main thermodynamic, statistical, and mechanical properties of the quark–gluon medium. In outline, their values found from 200 GeV data can be grouped as $T_{eq} \approx 360$ MeV, $T_{cr} \approx$ ≈ 170 MeV; $T_{dec} \approx 120$ MeV, $\tau_{therm} = \tau_{eq} \approx 0.6 < 1$ fm; $\tau_{dec} \approx 7$ fm, $e_{th} \approx 25$ GeV fm^{-3}, $e_{cr} \approx 1$ GeV fm^{-3}, $e_{dec} \approx 0.075$ GeB fm^{-3}, $s_{eq} \approx 110$ fm^{-3}, $\eta/s \approx 0.1$ ($1/4\pi$ in AdS/CFT); $n_B < 0.5$ fm^{-3}. These values show rapid thermalization, a high average initial energy density and quite a long 'lifetime' of the quark–gluon plasma before hadronization at rather low energy density and temperature predicted by lattice QCD. Complete thermalization in a time less than 1 fm is required to obtain the measured value of the elliptic flow and its centrality dependence, which is very sensitive to any deviation from the local thermal equilibrium of low-p_T particles. Collective excitations, resonances, and inelastic collisions keep the system in thermal equilibrium. The good agreement of the data with the ideal fluid dynamics points to a very small viscosity of QGP. Other transport coefficients (shear, diffusion, and heat conduction) are not important if the microscale defined by rescattering is much less than the macroscale related to medium expansion. A strong nonperturbative interaction should be responsible for its behavior as an ideal liquid: this is where the name of strong quark–gluon plasma (sQGP) comes from. In sQGP, for example, there may exist clusters [213] and colored bound states of massive quasiparticles [214] with heavier flavors. Resonance scattering on constituents of the quark–gluon medium can become important [215]. All that would give rise to a collective response of the medium with the new scales discussed above, the high pressure, large chromopermittivity, and long-range correlations necessary to explain the enhancement of strange parton production by nonlocal processes. The long 'lifetime' supports an approximate description of energy losses within an 'infinite' medium.

Hydrodynamics is presently an actively developing field. The main characteristics of low-p_T particles have been described in this approach. At the same time, many factors have to be taken into account, such as the thermodynamics, models of collective flows, the hadronization process, resonance decays, chemical composition, and the geometry of collisions. However, a fully consistent hydrodynamic description has not yet been found. Some controversial conclusions appear from time to time, for example, about the energy (from SPS to RHIC), the rapidity and centrality dependence of the elliptic flow, its absolute value, the transverse momentum dependence of various radii derived from HBT analysis, and the chemical composition of some species (e.g., the $\bar{p}/\pi$ ratio). It can be hoped that they will be resolved in the near future within the same set of fitting parameters. That would provide a deeper understanding of the collective thermodynamic and mechanical properties and evolution of the bulk matter.

5. Some new capabilities at the LHC

The first LHC experiments on pp interactions at 2.36 and 7 TeV already showed that even the most general characteristics like the inclusive pseudorapidity distributions in the central region $|\Delta\eta| < 2.4$ for the CMS (Compact Muon Solenoid) and $|\Delta\eta| < 1$ for ALICE (A Large Ion Collider Experiment) are not described by theoretical predictions well enough. Even though the qualitative features are reproduced, no Monte Carlo scheme (among the four tried) fits the results quantitatively. Surely, more surprises are waiting for us in correlation studies,[16] especially in heavy-ion experiments. The LHC energies open new possibilities for studies of the reviewed topics. Gluon–gluon processes will dominate. The formation length for the radiation of gluons (and photons) becomes larger at higher energies. Hence, high-energy partons feel the finite size of the interaction region. The spectra of radiated gluons and photons are predicted to become harder due to oscillations of the light-cone wave function [86, 216]. The emission from heavy quarks should be enhanced by the finite-size effects relative to light quarks. In general, the relative roles of surface effects, the initial high virtualities of the produced high-p_T partons, and the dead-cone effect in radiation by heavy quarks will be elucidated. Coherent final-state interactions must become stronger.

The smaller values of chromopermittivity for very high-energy partons discussed above indicates a weaker coupling and lower parton density of the medium at the LHC compared with the RHIC. Therefore, the role of fluctuations induced by instabilities will be enhanced at the LHC [217].

Both trigger and nontrigger experiments are important in AA collisions. Following the RHIC approach in trigger experiments, the partons (jets) at large angles with much higher energies will be available. Correspondingly, this allows studying jet quenching, ridge, and double-humped events in wider energy intervals. In particular, the energy dependence of the chromopermittivity may be found by studying by behavior of humps in wider energy intervals. Hump shifts due to the wake effect in semicentral collisions and due to a Lorentz transformation of the chromopermittivity tensor in a wide energy interval are of special interest.

In nontrigger experiments, studies of the response of the quark–gluon medium to extremely fast moving partons will be of primary importance. It would be quite instructive if events similar to the cosmic ray one are observed. Finite-size effects are especially important for forward-moving partons with large x.

The search for forward objects with a fixed mass [due to the transition radiation, Eqn (86)] or fixed transverse momentum [due to high-energy Cherenkov gluons, Eqn (91)] might be fruitful.

Effects due to Cherenkov gluons can be used to study the wide region of the (x, Q^2) plane available at the LHC. The

[16] The CMS Collaboration reported [218] an observation(!) of a ridge with a narrow distribution in the relative azimuthal angle and a broad distribution in the pseudorapidity difference in pp collisions at the energy 7 TeV.

different values of parton densities would correspond to different subregions on this plane.

The nonlinear effects described in Section 4.5 may become more pronounced, albeit still difficult to separate from the main effects due to the possible dispersive behavior of chromopermittivity.

More exotic experiments can be imagined. For example, triggers registering a single electron (positron) produced in a process of the convolution of a quark–antiquark pair, the inverse of those studied at e^+e^--colliders. The dielectric permittivity can be measured and formulas (63) and (66) compared with the data. Even though the cross section is very small, it might be measurable in the high-luminosity regime of the LHC.

6. Conclusions

The experimental studies at the SPS and, especially, the numerous and detailed data about heavy ion collisions at the RHIC provided us with invaluable information about a completely new field — the properties of the quark–gluon medium. They showed that AA events cannot be described as an additive collection of pp collisions. Heavy ion dynamics must take the collective behavior of the medium into account; this is clearly demonstrated by anisotropic flows, jet quenching, and peculiar correlations such as ridge and double-humped events.

Theoretical understanding of the medium evolution required the full-fledged application of QCD to speculate about such stages as the CGC, Glasma, thermalization, QGP, and hadronization. The specific configuration of fields in Glasma and consequences of deconfinement at the QGP stage need further studies. In turn, experimental results required reviving the theoretical methods widely applied in condensed matter physics. The modification of energy losses of partons in the medium due to formation length effects and its collective response (chromopermittivity) due to polarization are described in this manner. Hydrodynamics was extensively used for describing the collective behavior of this medium.

Both experimental and theoretical progress in this field are extremely fruitful and promising. Without a doubt, even more interesting results will be obtained in further searches at the RHIC. Exciting prospects have opened with the advent of the LHC in the new energy region.

Acknowledgments. This work was supported by the RFBR grants 09-02-00741, 08-02-91000-CERN, and the RAS–CERN program.

References

1. Iancu E, Venugopalan R, in *Quark-Gluon Plasma* (Eds R C Hwa, X-N Wang) (Singapore: World Scientific, 2004) p. 249; hep-ph/0303204
2. Venugopalan R, hep-ph/0412396
3. Leonidov A *Usp. Fiz. Nauk* **175** 345 (2005) [*Phys. Usp.* **48** 323 (2005)]
4. Gelis F et al. *Annu. Rev. Nucl. Part. Sci.* (2010), submitted; arXiv:1002.0333
5. McLerran L, hep-ph/0311028
6. McLerran L, Venugopalan R *Phys. Rev. D* **49** 2233 (1994)
7. McLerran L, Venugopalan R *Phys. Rev. D* **49** 3352 (1994)
8. McLerran L, Venugopalan R *Phys. Rev. D* **50** 2225 (1994)
9. Jeon S, Venugopalan R *Phys. Rev. D* **70** 105012 (2004)
10. Lappi T *Eur. Phys. J. C* **55** 285 (2008)
11. Kovner A, McLerran L, Weigert H *Phys. Rev. D* **52** 6231 (1995)
12. Fries R J, Kapusta J I, Li Y, nucl-th/0604054
13. Lappi T, McLerran L *Nucl. Phys. A* **772** 200 (2006)
14. Lappi T *Phys. Lett. B* **643** 11 (2006)
15. Venugopalan R, hep-ph/0412396
16. Matinyan S G, Müller B, Rischke D H *Phys. Rev. C* **57** 1927 (1998)
17. Fukushima K, Gelis F, McLerran L *Nucl. Phys. A* **786** 107 (2007)
18. Mueller A H, Son D T *Phys. Lett. B* **582** 279 (2004)
19. Romatschke P, Venugopalan R *Phys. Rev. Lett.* **96** 062302 (2006)
20. Romatschke P, Venugopalan R *Phys. Rev. D* **74** 045011 (2006)
21. Fujii H, Itakura K *Nucl. Phys. A* **809** 88 (2008)
22. Mrówczyński S *Phys. Lett. B* **214** 587 (1988)
23. Mrówczyński S *Phys. Lett. B* **314** 118 (1993)
24. Arnold P, Lenaghan J, Moore G D *JHEP* (08) 002 (2003)
25. Baier R et al. *Phys. Lett. B* **502** 51 (2001)
26. Arnold P, Moore G D *Phys. Rev. D* **73** 025006 (2006)
27. Mueller A H, Shoshi A I, Wong S M H *Nucl. Phys. B* **760** 145 (2007)
28. Khachatryan V *Nucl. Phys. A* **810** 109 (2008)
29. Jalilian-Marian J, Kovner A, Leonidov A, Weigert H *Phys. Rev. D* **59** 034007 (1999)
30. Iancu E, Leonidov A, McLerran L *Nucl. Phys. A* **692** 583 (2001)
31. Ferreiro E, Iancu E, Leonidov A, McLerran L *Nucl. Phys. A* **703** 489 (2002)
32. Weigert H *Nucl. Phys. A* **703** 823 (2002)
33. Balitsky I *Nucl. Phys. B* **463** 99 (1996)
34. Kovchegov Yu V *Phys. Rev. D* **61** 074018 (2000)
35. Gelis F, Lappi T, Venugopalan R *Phys. Rev. D* **78** 054019 (2008)
36. Gelis F, Lappi T, Venugopalan R *Phys. Rev. D* **78** 054020 (2008)
37. Gelis F, Lappi T, Venugopalan R *Phys. Rev. D* **79** 094017 (2009)
38. d'Enterria D, arXiv:0902.2011
39. Baier R, Schiff D, Zakharov B G *Annu. Rev. Nucl. Part. Sci.* **50** 37 (2000)
40. Kovner A, Wiedemann U A, in *Quark-Gluon Plasma* (Eds R C Hwa, X-M Wang) (Singapore: World Scientific, 2004) p.192
41. Gyulassy M, Vitev I, Wang X-N, Zhang B-W, in *Quark-Gluon Plasma* (Eds R C Hwa, X-N Wang) (Singapore: World Scientific, 2004) p.123
42. Zakharov B G *Nucl. Phys. B Proc. Suppl.* **146** 151 (2005); hep-ph/0412117
43. Casalderrey-Solana J, Salgado C A *Acta Phys. Polon. B* **38** 3731 (2007)
44. Wiedemann U A, arXiv:0908.2306
45. Majumder A, Van Leeuwen M, arXiv:1002.2206
46. Gribov V N, Lipatov L N *Yad. Fiz.* **15** 675 (1972) [*Sov. J. Nucl. Phys.* **15** 438 (1972)]
47. Altarelli G, Parisi G *Nucl. Phys. B* **126** 298 (1977)
48. Dokshitser Yu L *Zh. Eksp. Teor. Fiz.* **73** 1216 (1977) [*Sov. Phys. JETP* **46** 641 (1977)]
49. Belenky S Z *Lavinnye Protsessy v Kosmicheskikh Luchakh* (Shower Processes in Cosmic Rays) (Moscow: GITTL, 1948)
50. Dremin I M *Pis'ma Zh. Eksp. Teor. Fiz.* **31** 201 [*JETP Lett.* **31** 185 (1980)]
51. Dremin I M *Usp. Fiz. Nauk* **131** 715 (1980) [*Sov. Phys. Usp.* **23** 515 (1980)
52. Dremin I M, Leonidov A V *Yad. Fiz.* **35** 288 (1982) [*Sov. J. Nucl. Phys.* **35** 247 (1982)]
53. Dremin I M, Leonidov A V *Usp. Fiz. Nauk* **165** 759 (1995) [*Phys. Usp.* **38** 723 (1995)]
54. Leonidov A V, Ostrovsky D M *Yad. Fiz.* **60** 119 (1997) [*Phys. Atom. Nucl.* **60** 110 (1997)]
55. Leonidov A V, Ostrovsky D M *Yad. Fiz.* **62** 750 (1999) [*Phys. Atom. Nucl.* **62** 701 (1999)]
56. Zakharov B G *Pis'ma Zh. Eksp. Teor. Fiz.* **86** 509 (2007) [*JETP Lett.* **86** 444 (2007)]
57. Baier R et al. *Phys. Lett. B* **345** 277 (1995)
58. Baier R et al. *Nucl. Phys. B* **483** 291 (1997)
59. Baier R et al. *Nucl. Phys. B* **484** 265 (1997)
60. Baier R et al. *Phys. Rev. C* **58** 1706 (1998)
61. Gyulassy M, Lévai P, Vitev I *Nucl. Phys. B* **571** 197 (2000)
62. Gyulassy M, Levai P, Vitev I *Phys. Rev. Lett.* **85** 5535 (2000)
63. Gyulassy M, Levai P, Vitev I *Nucl. Phys. B* **594** 371 (2001)
64. Gyulassy M, Levai P, Vitev I *Phys. Lett. B* **538** 282 (2002)
65. Djordjevic M, Gyulassy M *Nucl. Phys. A* **733** 265 (2004)
66. Djordjevic M, Gyulassy M, Wicks S *Phys. Rev. Lett.* **94** 112301 (2005)

67. Wiedemann U A *Nucl. Phys. B* **588** 303 (2000)
68. Wiedemann U A *Nucl. Phys. B* **582** 409 (2000)
69. Wiedemann U A *Nucl. Phys. A* **690** 731 (2001)
70. Salgado C A, Wiedemann U A *Phys. Rev. D* **68** 014008 (2003)
71. Armesto N, Salgado C A, Wiedemann U A *Phys. Rev. D* **69** 114003 (2004)
72. Zakharov B G *Pis'ma Zh. Eksp. Teor. Fiz.* **63** 906 (1996) [*JETP Lett.* **63** 952 (1996)]
73. Zakharov B G *Pis'ma Zh. Eksp. Teor. Fiz.* **65** 585 (1997) [*JETP Lett.* **65** 615 (1997)]
74. Zakharov B G *Yad. Fiz.* **61** 924 (1998) [*Phys. Atom. Nucl.* **61** 838 (1998)]
75. Zakharov B G *Pis'ma Zh. Eksp. Teor. Fiz.* **70** 181 (1999) [*JETP Lett.* **70** 176 (1999)]
76. Guo X, Wang X-N *Phys. Rev. Lett.* **85** 3591 (2000)
77. Majumder A, Müller B *Phys. Rev. C* **77** 054903 (2008)
78. Arnold P, Moore G D, Yaffe L G *JHEP* (11) 057 (2001)
79. Arnold P, Moore G D, Yaffe L G *JHEP* (12) 009 (2001)
80. Arnold P, Moore G D, Yaffe L G *JHEP* (06) 030 (2002)
81. Turbide S et al. *Phys. Rev. C* **72** 014906 (2005)
82. Qin G-Y et al. *Phys. Rev. Lett.* **100** 072301 (2008)
83. Kämpfer B, Pavlenko O P *Phys. Lett. B* **477** 171 (2000)
84. Zakharov B G *Yad. Fiz.* **46** 148 (1987) [*Sov. J. Nucl. Phys.* **46** 92 (1987)]
85. Peigné S, Smilga A V *Usp. Fiz. Nauk* **179** 697 (2009) [*Phys. Usp.* **52** 659 (2009)]
86. Zakharov B G *Pis'ma Zh. Eksp. Teor. Fiz.* **80** 3 (2004) [*JETP Lett.* **80** 1 (2004)]
87. Armesto N et al. *JHEP* (02) 048 (2008)
88. Wang X-N, Huang Z, Sarcevic I *Phys. Rev. Lett.* **77** 231 (1996)
89. Sjöstrand T, Mrenna S, Skands P *JHEP* (05) 026 (2006)
90. Marchesini G et al. *Comput. Phys. Commun.* **67** 465 (1992)
91. Corcella G et al. *JHEP* (01) 010 (2001)
92. Corcella G et al., hep-ph/0210213
93. Lokhtin I P, Snigirev A M *Eur. Phys. J. C* **45** 211 (2006)
94. Zapp K et al. *Eur. Phys. J. C* **60** 617 (2009)
95. Armesto N, Cunqueiro L, Salgado C A *Eur. Phys. J. C* **63** 679 (2009)
96. Armesto N et al. *JHEP* (11) 122 (2009)
97. Leonidov A, Nechitailo V, arXiv:1006.0366
98. Bergmann G *Phys. Rep.* **107** 1 (1984)
99. Chakravarty S, Schmid A *Phys. Rep.* **140** 193 (1986)
100. Selikhov A V, Gyulassy M *Phys. Lett. B* **316** 373 (1993)
101. Selikhov A V, Gyulassy M *Phys. Rev. C* **49** 1726 (1994)
102. Zapp K, Stachel J, Wiedemann U A *Phys. Rev. Lett.* **103** 152302 (2009)
103. Zapp K, Stachel J, Wiedemann U A *Nucl. Phys. A* **830** 171c (2009)
104. Wang X-N, Guo X *Nucl. Phys. A* **696** 788 (2001)
105. Borghini N, Wiedemann U A, hep-ph/0506218
106. Lokhtin I P et al. *Comput. Phys. Commun.* **180** 779 (2009)
107. Dremin I M, Shadrin O S *J. Phys. G Nucl. Part. Phys.* **32** 963 (2006)
108. Armesto N, Pajares C, Quiroga-Arias P *Eur. Phys. J. C* **61** 779 (2009)
109. Shuryak E *Prog. Part. Nucl. Phys.* **62** 48 (2009)
110. Heinz U, hep-ph/0407360; CERN-2004-001
111. Dremin I M *Eur. Phys. J. C* **56** 81 (2008)
112. Djongolov M K, Pisov S, Rizov V *J. Phys. G Nucl. Part. Phys.* **30** 425 (2004)
113. Jackson J D *Classical Electrodynamics* (New York: Wiley, 1998) Fig. 7.9 [Translated into Russian (Moscow: Mir, 1965)]
114. Feynman R P, Leighton R B, Sands M *The Feynman Lectures on Physics* Vol. 1 (Reading, Mass.: Addison-Wesley, 1963) Ch. 31 [Translated into Russian (Moscow: Mir, 1967)]
115. Kalashnikov O K, Klimov V V *Yad. Fiz.* **31** 1357 (1980) [*Sov. J. Nucl. Phys.* **31** 699 (1980)]
116. Klimov V V *Yad. Fiz.* **33** 1734 (1981) [*Sov. J. Nucl. Phys.* **33** 934 (1981)]
117. Klimov V V *Zh. Eksp. Teor. Fiz.* **82** 336 (1982) [*Sov. Phys. JETP* **55** 199 (1982)]
118. Weldon H A *Phys. Rev. D* **26** 1394 (1982)
119. Blaizot J-P, Iancu E *Phys. Rep.* **359** 355 (2002)
120. Rebhan A, Romantschke P, Strickland M *Phys. Rev. Lett.* **94** 102303 (2005)
121. Rebhan A, Romantschke P, Strickland M *JHEP* (09) 041 (2005)
122. Arnold P, Moore G D, Yaffe L G *Phys. Rev. D* **72** 054003 (2005)
123. Qin G-Y et al. *Phys. Rev. Lett.* **103** 152303 (2009)
124. Koch V, Majumder A, Wang X-N *Phys. Rev. Lett.* **96** 172302 (2006)
125. Ruppert J *J. Phys. Conf. Ser.* **27** 217 (2005)
126. Zakharov B G *Pis'ma Zh. Eksp. Teor. Fiz.* **76** 236 (2002) [*JETP Lett.* **76** 201 (2002)]
127. Casalderrey-Solana J, Fernandez D, Mateos D, arXiv:0912.3717
128. Djordjevic M, Gyulassy M *Phys. Rev. C* **68** 034914 (2003)
129. Djordjevic M, Gyulassy M *Phys. Lett. B* **560** 37 (2003)
130. Djordjevic M *Phys. Rev. C* **73** 044912 (2006)
131. Goldberger M L, Watson K M *Collision Theory* (New York: Wiley, 1964) Ch. 11, sect. 3, sect. 4
132. Scadron M D *Advanced Quantum Theory and Its Applications Through Feynman Diagrams* (New York: Springer-Verlag, 1979) p. 326
133. Dremin I M *Pis'ma Zh. Eksp. Teor. Fiz.* **30** 152 (1979) [*JETP Lett.* **30** 140 (1979)]
134. Dremin I M *Yad. Fiz.* **33** 1357 (1981) [*Sov. J. Nucl. Phys.* **33** 726 (1981)]
135. Bolotovskii B M, Stolyarov S N *Usp. Fiz. Nauk* **114** 569 (1974) [*Sov. Phys. Usp.* **17** 875 (1975)]
136. Alfimov M, arXiv:1004.0286
137. Apanasenko A V et al. *Pis'ma Zh. Eksp. Teor. Fiz.* **30** 157 (1979) [*JETP Lett.* **30** 145 (1979)]
138. Kuzelev M V, Rukhadze A A *Metody Teorii Voln v Sredakh s Dispersiei* (Moscow: Fizmatlit, 2007); *Methods of Wave Theory in Dispersive Media* (Singapore: World Scientific, 2010)
139. Tamm I E, Frank I M *Dokl. Akad. Nauk SSSR* **14** 107 (1937) [*C.R. Acad. Sci. USSR* **14** 107 (1937)]; *Usp. Fiz. Nauk* **93** 388 (1967)
140. Grichine V M *Nucl. Instrum. Meth. Phys. Res. A* **482** 629 (2002)
141. Dremin I M, Kirakosyan M R, Leonidov A V, Vinogradov A V *Nucl. Phys. A* **826** 190 (2009)
142. Dremin I M *Mod. Phys. Lett. A* **25** 591 (2010)
143. Thoma M H, Gyulassy M *Nucl. Phys. B* **351** 491 (1991)
144. Arata N *Nuovo Cimento A* **43** 455 (1978)
145. Alexeeva K I et al. *Izv. Akad. Nauk SSSR. Ser. Fiz.* **26** 572 (1962)
146. Alekseeva K I et al. *J. Phys. Soc. Jpn.* **17** (A-III) 409 (1962)
147. Maslennikova N V et al. *Izv. Akad. Nauk SSSR. Ser. Fiz.* **36** 1696 (1972)
148. Dremin I M et al. *Yad. Fiz.* **52** 840 (1990) [*Sov. J. Nucl. Phys.* **52** 536 (1990)]
149. Adamovich M I et al. *J. Phys. G Nucl. Part. Phys.* **19** 2035 (1993)
150. Adamovich M I et al. *Eur. Phys. J. A* **5** 429 (1999)
151. Gogiberidze G L, Gelovani L K, Sarkisyan E K *Phys. Lett. B* **430** 368 (1998)
152. Gogiberidze G L, Gelovani L K, Sarkisyan E K *Phys. Lett. B* **471** 257 (1999)
153. Gogiberidze G L, Gelovani L K, Sarkisyan E K *Yad. Fiz.* **64** 147 (2001) [*Phys. Atom Nucl.* **64** 143 (2001)]
154. Dremin I M et al. *Phys. Lett. B* **499** 97 (2001)
155. Vokál S et al. *Yad. Fiz.* **71** 1423 (2008) [*Phys. Atom. Nucl.* **71** 1395 (2008)]
156. Ghosh D et al. *Can. J. Phys.* **86** 919 (2008)
157. Ghosh D et al. *Ind. J. Phys.* **82** 1339 (2008)
158. Wang F (STAR Collab.) *J. Phys. G Nucl. Part. Phys.* **30** S1299 (2004)
159. Wang F (STAR Collab.) *J. Phys. G Nucl. Part. Phys.* **34** S337 (2007)
160. Adams J et al. (STAR Collab.) *Phys. Rev. Lett.* **95** 152301 (2005)
161. Adler S S et al. (PHENIX Collab.) *Phys. Rev. Lett.* **97** 052301 (2006)
162. Adare A et al. (PHENIX Collab.) *Phys. Rev. Lett.* **101** 232301 (2008)
163. Adare A et al. (PHENIX Collab.) *Phys. Rev. C* **77** 011901(R) (2008)
164. Adare A et al. (PHENIX Collab.) *Phys. Rev. C* **78** 014901 (2008)
165. Ulery J G (STAR Collab.) *J. Phys. G Nucl. Part. Phys.* **35** 104032 (2008)
166. Ulery J G (STAR Collab.) *Int. J. Mod. Phys. E* **16** 3123 (2008); arXiv:0709.1633; arXiv:0801.4904
167. Pruneau C A *Phys. Rev. C* **79** 044907 (2009)
168. Jiangyong J *J. Phys. G Nucl. Part. Phys.* **35** 104033 (2008)
169. Jelley J V *Cherenkov Radiation and Its Applications* (New York: Pergamon Press, 1958) p. 13
170. Aggarwal M M et al. (STAR Collab), arXiv:1004.2377
171. Holzmann W G (PHENIX Collab.) *Nucl. Phys. A* **830** 781c (2009)
172. Ajitanand N N (PHENIX Collab.) *Nucl. Phys. A* **783** 519 (2007)

173. Abelev B I et al. (STAR Collab.) *Phys. Rev. Lett.* **102** 052302 (2009); arXiv:0912.3977
174. Armesto N et al. *J. Phys. G Nucl. Part. Phys.* **35** 054001 (2008)
175. Vitev I *Phys. Lett. B* **630** 78 (2005)
176. Stöcker H *Nucl. Phys. A* **750** 121 (2005)
177. Casalderrey-Solana J, Shuryak E V, Teaney D *J. Phys. Conf. Ser.* **27** 22 (2005)
178. Ruppert J, Müuller B *Phys. Lett. B* **618** 123 (2005)
179. Gubser S S, Pufu S S, Yarom A *JHEP* (09) 108 (2007)
180. Chesler P M, Yaffe L G *Phys. Rev. Lett.* **99** 152001 (2007)
181. Takahashi J et al. *Phys. Rev. Lett.* **103** 242301 (2009)
182. Andrade B P G et al., arXiv:0912.0703
183. Hama Y et al., arXiv:0911.0811
184. Betz B et al. *Phys. Rev. C* **79** 034902 (2009)
185. Shuryak E *J. Phys. G Nucl. Part. Phys.* **35** 104044 (2008)
186. Polosa A D, Salgado C A *Phys. Rev. C* **75** 041901(R) (2007)
187. Voloshin S A *Nucl. Phys. A* **749** 287 (2005)
188. Chiu C B, Hwa R C *Phys. Rev. C* **74** 064909 (2006)
189. Dremin I M et al. *J. Phys. G Nucl. Part. Phys.* **35** 095106 (2008)
190. Azarkin M, Diploma Work (Moscow: MEPhT, 2010)
191. Dremin I M, Nechitailo V A *Int. J. Mod. Phys. A* **24** 1221 (2009)
192. Arnaldi R et al. (NA60 Collab.) *Phys. Rev. Lett.* **96** 162302 (2006)
193. Trnka D et al. (CBELSA/TAPS Collab.) *Phys. Rev. Lett.* **94** 192303 (2005)
194. Naruki M et al. *Phys. Rev. Lett.* **96** 092301 (2006)
195. Muto R et al. (KEK-PS E325 Collab) *Phys. Rev. Lett.* **98** 042501 (2007)
196. Kozlov A (PHENIX Collab.) *Eur. Phys. J. A* **31** 836 (2007)
197. Kotulla M (CBELSA/TAPS Collab.) *AIP Conf. Proc.* **870** 506 (2006)
198. Dremin I M et al. *J. Phys. G Nucl. Part. Phys.* **35** 095106 (2008)
199. Dremin I M *Int. J. Mod. Phys. A* **22** 3087 (2007)
200. Ryazanov M I *Elektrodinamika Kondensirovannykh Sred* (Moscow: Nauka, 1984) p. 210
201. Chakraborty P, Mustafa M G, Thoma M H *Phys. Rev. D* **74** 094002 (2006)
202. Chakraborty P et al. *J. Phys. G Nucl. Part. Phys.* **34** 2141 (2007)
203. Ginzburg V L, Frank I M *J. Phys. USSR* **9** 353 (1945); *Zh. Eksp. Teor. Fiz.* **16** 15 (1946)
204. Dremin I M, arXiv:1003.2145
205. Kirakosyan M R, Leonidov A V, arXiv:0810.5442
206. Tamm I E *J. Phys. USSR* **1** 439 (1939) [Translated into Russian: *Sobranie Nauchnykh Trudov* Vol. 1 (Moscow: Nauka, 1975) p. 77]
207. Dremin I M *Yad. Fiz.* **73** 684 (2010) [*Phys. Atom. Nucl.* **73** 657 (2010)]
208. Rukhadze A A *Zh. Tekh. Fiz.* **62** 669 (1962)
209. Ter-Mikaelian M L *Vliyanie Sredy na Elektromagnitnye Protsessy pri Vysokikh Energiyakh* (High-Energy Electromagnetic Processes in Condensed Matter) (Erevan: Izd. AN ArmSSR,1969) [Translated into English (New York: Wiley-Intersci., 1972)]
210. Aleksandrov A F, Rukhadze A A *Lekzii po Elektrodinamike Plazmopodobnykh Sred; Neravnovesnye Sredy* (Moscow: Izd. MGU, 2002) p. 112
211. Silin V P, Rukhadze A A *Elektromagnitnye Svoistva Plazmy i Plazmopodobnykh Sred* (Moscow: Gosatomizdat, 1961) p. 173
212. Ginzburg V L *Rasprostranenie Elektromagnitnykh Voln v Plazme* (The Propagation of Electromagnetic Waves in Plasmas) (Moscow: Nauka, 1967) [Translated into English (Oxford New York: Pergamon Press, 1970)]
213. Yukalov V I, Yukalova E P *Physica A* **243** 382 (1997)
214. Shuryak E V, Zahed I *Phys. Rev. D* **70** 054507 (2004)
215. Rapp R et al. *Nucl. Phys. A* **830** 861c (2009)
216. Aurenche P, Zakharov B G *Pis'ma Zh. Eksp. Teor. Fiz.* **90** 259 (2009) [*JETP Lett.* **90** 237 (2009)]
217. Mrówczyński S *Acta Phys. Polon. B* **39** 1665 (2008); arXiv:0804.0275
218. Khachatryan V et al. (CMS Collab.) *JHEP* (09) 091 (2010)